IMPLEMENTATION AND VALIDATION OF TURBULENCE MODELS IN UNS2D CODE

PROJECT REPORT

Submitted by

VATTI SANDEEP(SC07B103)

YASHWANTH KUMAR NAKKA (SC07B108)

FOR THE AWARD OF DEGREE
OF
BACHELOR OF TECHNOLOGY

IN
AEROSPACE ENGINEERING

FEB-MAY, 2011

INDIAN INSTITUTE OF SPACE SCIENCE AND TECHNOLOGY
THIRUVANANTHAPURAM

CERTIFICATE

This is to certify that this project report entitled "Implementation and validation of Turbulence model in UNS2D code" is a bonafide record of work done by Vatti Sandeep and Yashwanth Kumar Nakka under my supervision at VSSC from 6th Feb to 30th May2011, in partial fulfillment of the requirements for the award of Degree of Bachelor of Technology of the Indian Institute of Space Science and Technology, Thiruvananthapuram**.**

Dr. C. Unnikrishnan
Sci. /Eng., F
Aerodynamic R&D Division
Aeronautics Entity
VSSC

V. Ashok
Divisional Head
Aerodynamics R&D Division
Aeronautics Entity
VSSC

Place: Thiruvananthapuram
Date: 2-06-2011

ACKNOWLEDGEMENT

We would like to whole heartedly thank our guide Shri. Dr. C. Unnikrishnan, Sci. /Eng. F, ARD, for his untiring support and encouragement, and invaluable guidance throughout the project period. Without the kind of help he extended, the project would not have been realized. We would also like to thank Shri. Dr.V.Ashok, Head ARD & Shri. Uday Bhaskar Sci. /Eng. C, ARD for their support. We would also like to thank our IIST Project Supervisor – Shri. Pankaj Priyadarshi for his valuable suggestions and support. We are also thankful to our college for giving us this opportunity and management staff for their support.

ABSTRACT

Eddy viscosity turbulence models have been implemented in the UNS2D code. Algebraic turbulence models – Baldwin Lomax and Johnson and King, its modifications are implemented. A two-equation turbulence model k-ε with Chien's near wall damping functions is implemented. The above models have been used to simulate the turbulent supersonic flow over a flat plate and transonic flow over an axis-symmetric bump. The results obtained are compared against available experimental and computational data and problems encountered are discussed. Spalart-Allmaras model which has already been implemented is also validated along with the above models for both the test cases.

NOMENCLATURE

u	- x-direction velocity
v	- y-direction velocity
$-\rho\overline{u'v'}$	- Reynolds Shear stress
μ	- Molecular Viscosity
μ_T	-Turbulent eddy viscosity
Pr	- Prandtl Number
Pr_T	- Turbulent Prandtl number
ω	- Vorticity
ρ	- Density
Cf	- Coefficient of Friction
Cd	- Coefficient of Drag
Ch	- Stanton Number
Cp	- Coefficient of Pressure
M	- Mach number
Re	- Reynolds Number
k	-Specific turbulence kinetic energy
ε	- Turbulence dissipation rate
y	- Co-ordinate normal to solid surface
τ	- Local shear stress
u_τ	- Friction velocity
δ	- Boundary layer thickness
U_e	-velocity at the edge of the boundary layer
D	- near wall damping term
c	- chord length of arc bump
p	-Pressure

e - Internal energy

∇ - Gradient vector

V - Velocity vector

c_∞ - Free stream velocity of sound

Subscripts:

eq - equilibrium conditions

m - Values of quantities of where $-\rho\overline{u'v'}$ is maximum

∞ - Free stream conditions

Superscripts:

$( )'$ - Fluctuating quantities

$\overline{( )}$ - Time averaged quantities

CONTENTS

LIST OF FIGURES:

LIST OF TABLES

1. INTRODUCTION

Most of the flows we encounter in our daily life are turbulent. Although a precise definition for turbulence cannot be given, turbulent flow features certain characteristics. It is highly irregular, high diffusivity, large Reynolds numbers, three dimensional, high dissipation etc.. Turbulence significantly affects the drag, heat transfer rate. Hence it is very essential to model turbulence in the flow to accurately predict these parameters. The physics of the turbulence is not yet fully understood. The inherent random nature of the flow makes the prediction very difficult. The equations used for solving of laminar flow cannot be used for solving turbulence because they cannot accommodate for the perturbations in the flow and hence Reynolds averaged Navier-Stokes equations are used. Direct numerical simulation is still not computationally efficient to predict turbulence, because of the very fine mesh needed to resolve the tiniest of the turbulent scales. This results in huge memory and processor requirements for the simplest geometry and flow that we can think of. Hence turbulent models have been developed to simulate the effects of the turbulence on the flow regime. Many families of models like Eddy Viscosity models, detached eddy models, large eddy models exist. Eddy viscosity models are the most popular because of their simplicity in implementation and accurate flow prediction. In this project various eddy viscosity models of different complexities are implemented and are tested in UNS2D code.

UNS2D is a Reynolds Averaged Thin layer Navier Stokes solver available in ARD, VSSC. Two turbulence models – Baldwin Lomax and Spalart-Allmaras were already implemented in the code. The code is finite volume code using state of the art modern techniques like upwind differencing, flux-vector splitting, and multi-grid methods for obtained good results.

The implementation of the model requires adding additional subroutines to the existing code, as well as modifying the existing code, other sub-routines (if required). The code is written in FORTRAN77.

About Centre:

The project was done in Aerodynamics Research Division (ARD), in Aeronautics Entity, VSSC. The division deals with research in Aerodynamic field, development of CFD software, implementation of new turbulence models and computational analysis of aerodynamic configurations for VSSC, ISRO.

Aims and Objectives:

1. Implementation and validation of Baldwin-Lomax algebraic turbulence model.
2. Implementation and validation of Johnson-Kind half-equation turbulence model and its variants.
3. Implementation and testing of k-ε two equation turbulence model
4. Validation of Spalart-Allmaras and above implemented turbulence models.

Brief theoretical background:

Turbulence modeling is done to solve the turbulence closure problem. To model turbulence properly all the length and time scales involved in the turbulent flow field must be resolved. As mentioned above there are different families of turbulence models like eddy viscosity models, Reynolds shear stress model. Eddy viscosity models are most widely used turbulence models because of their computational simplicity. In eddy viscosity models the Reynolds shear stress are linked to the velocity gradients via turbulence viscosity, this is called Boussinesq assumption, where the Reynolds stress tensor in the time averaged Navier stokes equations is replaced by turbulent viscosity multiplied by the velocity gradients.

$$-\rho\overline{u'v'} = \mu_t\left(\frac{\partial u}{\partial y} + \frac{dv}{dx}\right)$$

The above assumption gives good results even though turbulence is not a property of fluid but a property of the flow. Description of turbulence with turbulence eddy viscosity is due the resemblance in the effects of turbulence fluctuations to random molecular fluctuations that cause viscosity. Algebraic turbulence models use the prandtl's mixing length assumption, where in eddy viscosity is model to be a product of some length scale and velocity scale. In one equation turbulence model, a transport is equation is model for a turbulent quantity (usually turbulent kinetic energy) and the second turbulent quantity is calculated from an algebraic expression. The two turbulence quantities are used to find the length scales and time scales in the flow, using which eddy viscosity is calculated. In two equation eddy viscosity models, eddy viscosity is calculated from two scalars generally turbulent kinetic energy and its dissipation which are obtained solving the two modeled equations.

2. IMPLEMENTATION OF ALGEBRAIC TURBULENCE MODELS

2.1 BALDWIN-LOMAX TURBULENCE MODEL

Introduction:

Baldwin-Lomax (B-L) is a zero-equation eddy viscosity based turbulence model developed in 1964. It is one of the earliest turbulence models developed when multi equation turbulence models are still in its infancy and computational power is very low. The model is best suited for high speed flows with thin attached boundary layers, but fares relatively poor in cases with large separated regions. Although more efficient algorithms like one-equation Spalart-Allmaras and two-equation *k-ε* and *k-ω* models are available, Baldwin-Lomax model is still used widely when quick results are needed with sufficiently accurate results rather than accurate flow prediction. B-L model can be used with both two-dimensional and three dimensional flows. In this present report two dimensional implementation of the model in UNS2D code has been discussed.

Turbulence Model:

Baldwin Lomax is a two layer turbulence model, which gives eddy-viscosity as a function of flow parameters and boundary layer profile. The basic equations considered are the Navier-Stokes equations with turbulence being simulated by the usage of the eddy viscosity. The molecular viscosity μ is replaced by $\mu+\mu_t$ and heat flux terms k/c_p is replaced by $\mu/Pr + \mu_t/Pr_t$.Unlike the Cecebi-Smith turbulence model, which requires an approximation of initial boundary layer profile, B-L model doesn't require one. This has been achieved by the usage of a cross over distance using two different formulations in the outer and inner layers of the flow (closer to wall).

$$\mu_T = \begin{cases} (\mu_T)_{inner} & y \leq y_{crossover} \\ (\mu_T)_{outer} & y > y_{crossover} \end{cases}$$

Where y is the normal distance of the cell from the wall and $y_{crossover}$ is the smallest value of y at which values from inner and outer layers become equal. The Baldwin-Lomax turbulence model equations are non-dimensionlized and have been used for calculations as follows.

In the inner layer Prandtl-Van Driest formulation is used.

$$(\mu_t)_{inner} = \rho l^2 |\omega|$$

Where

$$l = ky\left[1 - exp\left(-\frac{y^+}{A^+}\right)\right] y^+ = \frac{\left(\sqrt{\rho_w \tau_w}\right)}{\mu_w} y \frac{M_\infty}{Re_\infty}$$

$|\omega|$is the magnitude of vorticity given by

$$|\omega| = \sqrt{\left(\frac{\partial u}{\partial y} - \frac{\partial v}{\partial x}\right)^2}$$

Clauser formulation has been used for outer layer, where

$$\mu_t = KC_{CP}\rho F_{WAKE} F_{KLEB}(y)$$

$$F_{WAKE} = \begin{Bmatrix} y_{MAX} F_{MAX} \\ or \\ C_{WK} y_{MAX}\, u_{DIF}^2 / F_{MAX} \end{Bmatrix} the\ smaller\ one$$

Fmax and corresponding Ymax can be calculated from the maximum of F(y)

$$F(y) = y|\omega|[1 - exp(-y^+/A^+)]$$

F_{KLEB}– Klebanoff intermittency factor can be calculated by

$$F_{KLEB}(y) = \left[1 + 5.5\left(\frac{C_{KLEB} y}{y_{max}}\right)^6\right]^{-1}$$

$$U_{DIF} = \left(\sqrt{u^2 + v^2}\right)_{MAX} - \left(\sqrt{u^2 + v^2}\right)_{MIN}$$

The transition to turbulence is simulated by taking

$$\mu_T = 0 \quad if \quad (\mu_T)_{\max(i)} < C_{MUTM}\mu_\infty$$

Constants:

$$A^+ = 26 \quad C_{CP} = 1.6 \quad C_{KLEB} = 0.3 \quad C_{WK} = 0.25 \quad k = 0.4 \quad K = 0.0168 \quad P_r = 0.72$$

$$P_{rt} = 0.9 \quad C_{MUTM} = 14$$

Implementation:

1. The model has been implemented as a subroutine which takes flow variables and geometric variables as input and returns turbulent momentum and energy multiplication factors as outputs.
2. The values of all the inner layer eddy viscosity and outer layer are calculated across the flow in separate loops.
3. The minimum of the two eddy viscosities and corresponding cross-over point are found. (In the inner cells inner layer eddy viscosity will minimum as compared to outer layer eddy viscosity and vice-versa.)
4. The maximum of the eddy viscosity thus obtained in a separate loop, and compared with the $C_{MUTM}\mu_{\infty}$. If the maximum of the eddy viscosity if found less than the constant, the eddy viscosities across the flow for the given stream wise location is set to zero. The point where maximum eddy viscosity crosses the constant becomes the transition point to turbulence.
5. The obtained final eddy viscosities at the cells are then used to find the momentum and energy viscosity multiplication factors using the following relations.

2.2 JOHNSON AND KINGS TURBULENCE MODEL

Introduction:

The Johnson and King model is a half-equation model turbulence model. The model has a assumed eddy viscosity distribution that has its velocity scale as the maximum Reynolds shear stress. The influence of history effects are modeled by using an ordinary differential equation derived from the turbulent kinetic energy equation (see Ref. [6],[9]) to describe the stream wise development of the maximum Reynolds shear stress. In the outer part of the boundary layer, the eddy viscosity is treated as a free parameter which is adjusted in order to satisfy the ODE for the maximum shear stress. Because of this, the model is not simply an eddy viscosity model, but contains features of a Reynolds stress model. It is composed of an algebraic eddy viscosity equation and a differential equation. The scaling of outer part of the boundary layer takes into account the non-equilibrium effects when the flow changes rapidly, as in the case of a strong adverse pressure gradient. Non-equilibrium conditions occur when the turbulence production no longer equals the turbulent dissipation energy. Under these conditions the traditional eddy viscosity models fail to correctly predict the actual flow

physics. The Johnson and King model is specifically intended to model flows with strong adverse pressure gradients or flows where separation is present. It is in these flow regimes that nonequilibrium effects must be accounted for and properly modeled.

Turbulence model:

The formulation of Johnson and kings model is as follows:

The equation for eddy viscosity is given by:

$$\vartheta_t = \vartheta_{to}(1 - exp\frac{-\vartheta_{ti}}{\vartheta_{to}})$$

Where ϑ_{to} and ϑ_{ti} are outer and inner viscosities respectively and are defined by,

$$\vartheta_{to} = \sigma(x)KU_e\delta^*\gamma$$

$$\vartheta_{ti} = \kappa D^2 u_s y$$

$U_e\delta^*$ can be found using the following equation.

$$U_e\delta^* = \int_0^\delta y|\omega|dy$$

For high Reynolds number vorticity decrease very rapidly with increasing distance from the wall. Thus the integral can be evaluated using a course approximation of δ, which can be taken as the first normal distance from the wall where ω is less than $\varepsilon\omega_{max}$, ε is a very small number. Boundary layer thickness can be approximated as follows:

$$\delta = 1.2y_{1/2} \quad where\ y_{1/2} = y\ at\ \frac{F}{F_{max}} = 0.5\ ;\ \ F = y|\omega|$$

In the above equation, U_e edge of the boundary layer velocity, γ is klebanoffs intermittency factor, δ boundary layer thickness, D is near wall damping term, u_s maximum Reynolds shear stress.

$$u_s = \overline{(-u'v')_m}^{-0.5}$$

The subscript m indicates that the variable is evaluated at the y location where the Reynolds shear stress is a maximum. The maximum shear stress location will vary in the stream wise

direction. The value of A+ is 15, K is 0.0168, and that of von Karman's constant, κ, is 0.40. The Johnson and kings model requires the solution of following differential equation:

$$\overline{u_m}\frac{\partial g}{\partial x}+\frac{a_1}{2L_m}\left[\left(\frac{g}{g_{eq}}-1\right)-\frac{C_{diff}\,L_m\left|1-\sigma(x)^{\frac{1}{2}}\right|}{a_1[0.7\delta-y_m]}\right]=0$$

Where $g_{eq}=\overline{(-u'v')_{eq,m}}^{-0.5}$ and $g=\overline{(-u'v')_m}^{-0.5}$ .g_{eq} is equilibrium Reynolds shear stress. The ODE was solved using Euler implicit scheme. In the above equation C_{dif} and a_1 are modeling constants and taken as 0.5 and 0.25 respectively. The length scale L_m is based on the maximum Reynolds shear stress height for inner region and on the boundary layer thickness for outer region.

$$L_m=0.4y_m\frac{y_m}{\delta}\leq 0.225$$

$$L_m=0.09\delta\quad\frac{y_m}{\delta}>0.225$$

The above differential equation is used to control the value of σ at each stream wise location in the flow. Therefore the value ϑ_{to} is affected by by the solution of the differential equation. This makes the outer eddy viscosity strongly dependent on the development of the Reynolds shear stress instead of just the mean velocity profile. The eddy viscosity model is used to determine the shear stress and the ODE is then used to control the level of the shear stress through the σ parameter. The n+1 iteration value of σ is calculated using the following method at each stream wise location

$$\sigma(x)^{n+1}=\sigma(x)^n\frac{\tau_{m,ODE}}{\tau_{m,actu\,al}}$$

$$\tau_m=\overline{(-u'v')_m}^{0.5}$$

Implementation:

The Johnson-kings model was implemented (see Ref.[9]) as the subroutine in UNS2D solver. Inputs to the subroutine are geometric data, flow variables and turbulence viscosity of previous iteration.

The values of$\sigma(x)$, g_{eq}, g are stored from previous iteration. The value of $\sigma(x)$ is initialized as 1.

1. Boundary layer parametersU_e, δ^*,δ are calculated.
2. Reynolds shear stress $\overline{(-u'v')_m}$ is calculated using the previous value of ϑ_t.
3. Compute, u_m,y_m, L_m at each stream wise location, at y location where $\overline{(-u'v')}$ is maximum
4. Calculate equilibrium Reynolds shear stress$\overline{(-u'v')_{eq,m}}$. It can be calculated from equilibrium eddy viscosity models like Baldwin Lomax or can be calculated from the above model, by using $\sigma(x)$=1, the values g_{eq} are stored at this point.
5. Solve the differential equation for g. Store values of g at this point.
6. Compute new $\sigma(x)$ values.
7. Calculate the new eddy viscosityϑ_t, use the value of $\overline{(-u'v')_m}$ found in (3) for the u_s term.

2.3 MODIFIED JOHNSON AND KINGS TURBULENCE MODEL

In modified Johnson and kings turbulence model (see Ref. [13]) the term u_s is modified for better shock capture and for improving the reattachment point and the viscous effects after the reattachment point for separated flows. A+=17

$$u_s = \sqrt{\frac{\rho_w}{\rho}}u_\tau(1-\gamma_2) + \sqrt{\frac{\rho_m}{\rho}}\gamma_2 u_m$$

$$\gamma_2 = 1 - \exp\left(-\frac{y}{L_c}\right)$$

$$L_c = \frac{\sqrt{\rho_w}u_\tau}{\sqrt{\rho_w}u_\tau + \sqrt{\rho_m}u_m}L_m$$

$$u_m = \overline{(-u'v')_m}^{0.5}$$

u_τ, is the wall shear velocity.

2.4 JOHNSON AND ABID TURBULENCE MODEL

The viscosity distribution used in this model is same as that of Johnson and kings turbulence model i.e,

$$\vartheta_t = \vartheta_{to}(1 - exp\frac{-\vartheta_{ti}}{\vartheta_{to}})$$

Following modifications (see Ref. [18]) were made in Johnson and kings model to avoid calculation of boundary layer parameters. The inner and outer eddy viscosities are:

$$\vartheta_{to} = \sigma(x)KC_cF_w\gamma_k$$

$$\vartheta_{ti} = \kappa D^2 u_s y$$

$$u_s = \overline{(-u'v')_m}^{-0.5}$$

$$C_c = 1.6, A+= 17, F_w = N_{max}\,F_{max}$$

F_{max} is the maximum of the function $F = y|\omega|D$ and N_{max} is the body normal distance at which F is maximum.

$$\gamma_k = \left[1 + 5.5\left(\frac{0.3y}{N_{max}}\right)^6\right]^{-1}$$

Boundary layer thickness is approximated as $\delta = 1.9N_{max}$

$$L_m = \min(0.4y_m, 0.09\delta)$$

Implementation of the above model is similar to that of Johnson and kings model.

Flow chart – Johnson-king

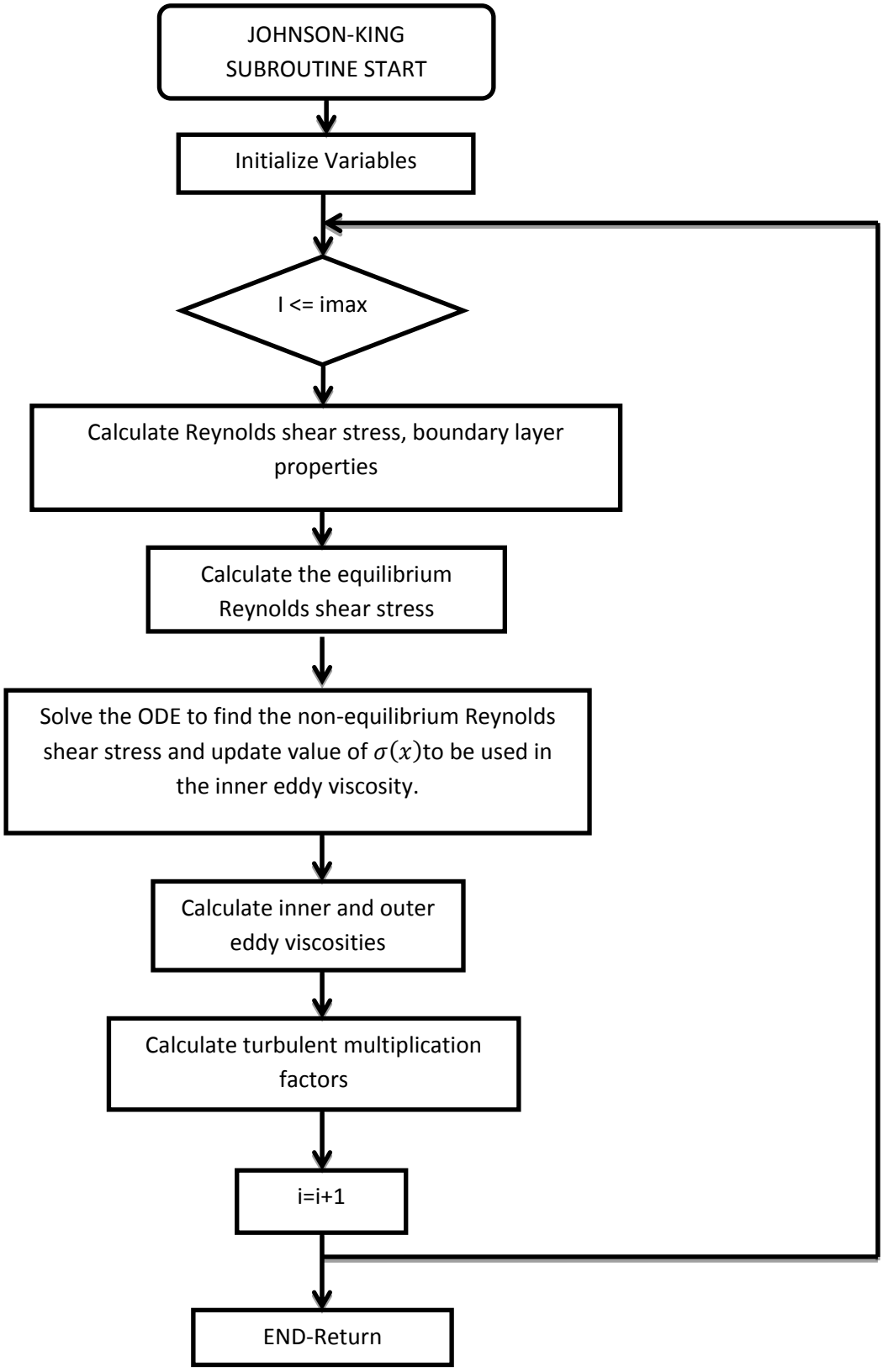

Flow chart – Baldwin Lomax

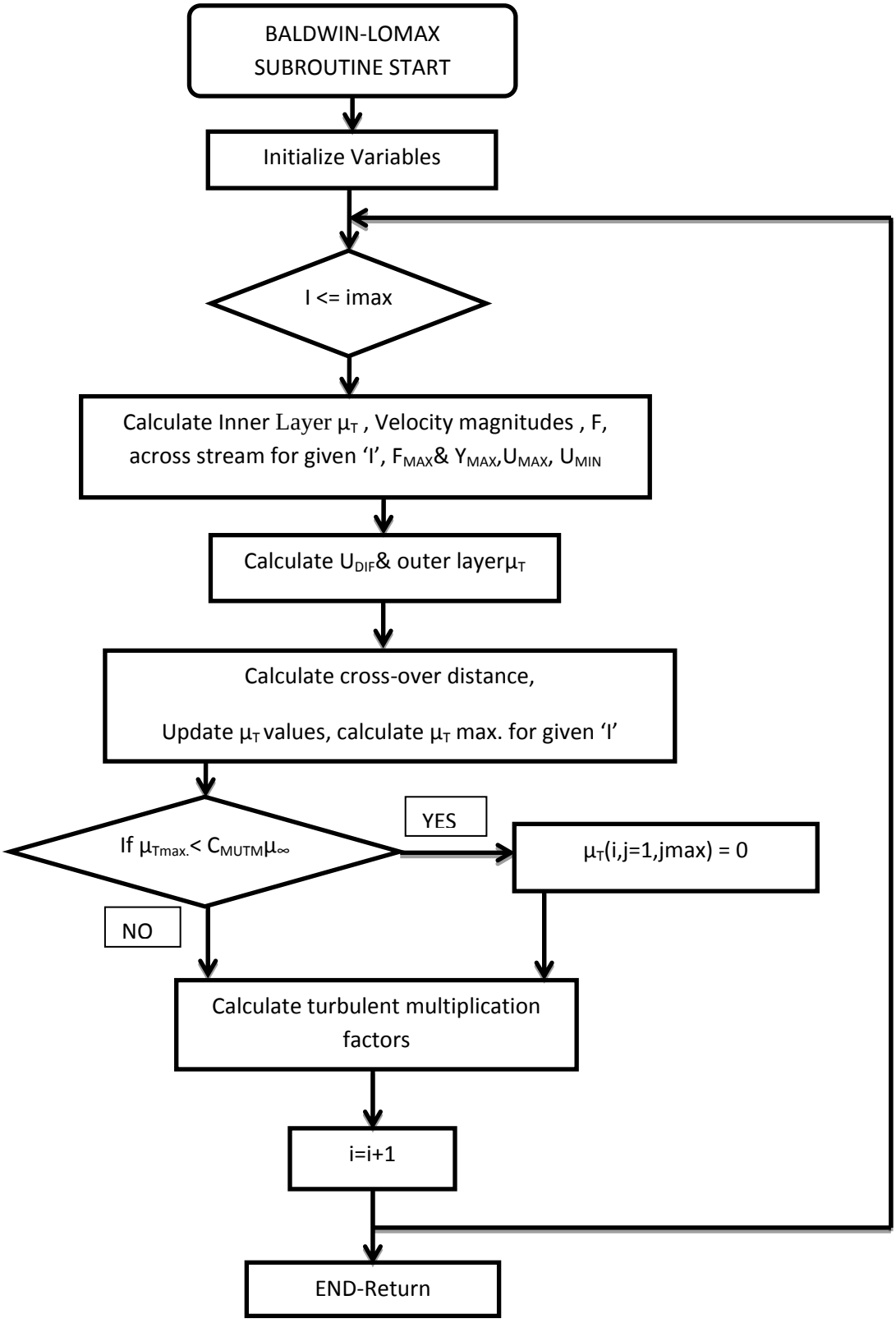

3. IMPLEMENTATION OF K-EPSILON TURBULENCE MODEL

3.1 INTRODUCTION

k-ε is one of the oldest and most popular two equation eddy viscosity turbulence model. It involves the calculation of two additional scalar transport equations for kinetic energy and its dissipation rate. The eddy viscosity is then a function of these two scalars. The obtained eddy viscosity is used to calculate the Reynolds Stress Tensor, which is approximated as a function of eddy viscosity and velocity gradients – the Boussinesq assumption. *k-ε* model with Chien's near wall functions is used for the implementation.

3.2 TURBULENCE MODEL

Reynolds Averaged equations have been used for the turbulence modeling. In addition to the four flow equations – conservation of mass, momentum and energy equations, two more equations are solved for the calculation of specific turbulence kinetic energy and turbulent energy dissipation rate.

$$\frac{\partial(\rho k)}{\partial t}+\frac{\partial(\rho k u_i)}{\partial x_i}=\frac{\partial}{\partial x_i}\left[\left(\mu+\frac{\mu_t}{\sigma_k}\right)\frac{\partial k}{\partial x_j}\right]+P_k-\rho\varepsilon+\varphi_k$$

$$\frac{\partial(\rho \varepsilon)}{\partial t}+\frac{\partial(\rho \varepsilon u_i)}{\partial x_i}=\frac{\partial}{\partial x_i}\left[\left(\mu+\frac{\mu_t}{\sigma_\varepsilon}\right)\frac{\partial \varepsilon}{\partial x_j}\right]+C_{1\varepsilon}(P_k)-C_{2\varepsilon}\rho\frac{\varepsilon^2}{k}+\varphi_\varepsilon$$

The above equations are non-dimensionalized using:

$$x^*=x/L_r\ y^*=y/L_r u^*=u/c_\infty\ v^*=v/c_\infty$$

$$t^*=\frac{t}{(L_r/c_\infty)}\rho^*=\rho/\rho_\infty\ T^*=T/T_\infty\ p^*=\frac{p}{\rho_\infty c_\infty^2}$$

$$E^*=\frac{E}{\rho_\infty c_\infty^2}\mu^*=\mu/\mu_\infty\ \mu_T^*=\mu_T/\mu_\infty\ k^*=\frac{k}{c_\infty^2}\varepsilon^*=\frac{\varepsilon}{(c_\infty^3/L_r)}$$

The resulted dimensionless equations are as follows

$$\frac{\partial(\rho k)}{\partial t}+\frac{\partial(\rho k u_i)}{\partial x_i}=\frac{M_\infty}{Re_\infty}\frac{\partial}{\partial x_i}\left[\left(\mu+\frac{\mu_t}{\sigma_k}\right)\frac{\partial k}{\partial x_j}\right]+P_k-\rho\varepsilon+\varphi_k$$

$$\frac{\partial(\rho \varepsilon)}{\partial t}+\frac{\partial(\rho \varepsilon u_i)}{\partial x_i}=\frac{M_\infty}{Re_\infty}\frac{\partial}{\partial x_i}\left[\left(\mu+\frac{\mu_t}{\sigma_\varepsilon}\right)\frac{\partial \varepsilon}{\partial x_j}\right]+C_{1\varepsilon}(P_k)-C_{2\varepsilon}\rho\frac{\varepsilon^2}{k}+\varphi_\varepsilon$$

(* is omitted non-dimensional parameters for the sake of simplicity, and the following equations are all in non-dimensionalized form)

The governing equations for the flow – Navier Stokes and the turbulence transport equations can be represented in the following form –

$$\frac{\partial U}{\partial t} + \frac{\partial (F - F_v)}{\partial x} + \frac{\partial (G - G_v)}{\partial y} = Q$$

where, *U* is the flow variable matrix, *F* and *G* are their corresponding inviscid flux vectors

$$U = \begin{pmatrix} \rho \\ \rho u \\ \rho v \\ E \\ \rho k \\ \rho \varepsilon \end{pmatrix} \qquad F = \begin{pmatrix} \rho u \\ \rho u^2 + p \\ \rho v u \\ (E + p)u \\ \rho k u \\ \rho \varepsilon u \end{pmatrix} \qquad G = \begin{pmatrix} \rho v \\ \rho u v \\ \rho v^2 + p \\ (E + p)u \\ \rho k v \\ \rho \varepsilon v \end{pmatrix}$$

$$E = \rho e + \frac{\rho \bar{V} \bar{V}}{2} + \rho k$$

F_v and G_v are viscous flux vectors

$$F_v = \begin{pmatrix} 0 \\ \tau_{xx} - (2/3)\rho k \\ \tau_{xy} \\ u\tau_{xx} + v\tau_{xy} - q_x - (2/3)\rho k u \\ \mu_k (\partial k / \partial x) \\ \mu_\varepsilon (\partial \varepsilon / \partial x) \end{pmatrix}$$

$$G_v = \begin{pmatrix} 0 \\ \tau_{xy} \\ \tau_{yy} - (2/3)\rho k \\ u\tau_{xy} + v\tau_{yy} - q_y - (2/3)\rho k v \\ \mu_k (\partial k / \partial y) \\ \mu_\varepsilon (\partial \varepsilon / \partial y) \end{pmatrix}$$

$$\mu_k = 1 + \frac{\mu_T}{\sigma_k} \qquad \mu_\varepsilon = 1 + \frac{\mu_T}{\sigma_\varepsilon}$$

$$\sigma_k = 1.0 \qquad \sigma_\varepsilon = 1.3$$

The viscosity μ is calculated from Sutherland's formula

$$\mu = \frac{(1+S)T^{3/2}}{(T+S)}$$

Where, *T* is the temperature at the cell and *S* is 110.4/288.15

Q is the source term:

$$Q = \begin{pmatrix} 0 \\ 0 \\ 0 \\ 0 \\ P - \rho\varepsilon - 2\frac{M_\infty}{Re_\infty}\mu\frac{k}{y_n^2} \\ c_1\frac{\varepsilon}{k}P - c_2\frac{\rho\varepsilon^2}{k} - 2\frac{M_\infty}{Re_\infty}\mu\frac{\varepsilon}{y_n^2}e^{-y^+/2} \end{pmatrix}$$

$$c_1 = 1.44 \quad c_2 = 1.92\left(1 - 0.22e^{-Re_T^2/36}\right) \quad Re_T = \frac{\rho k^2}{\mu\varepsilon}\frac{Re_\infty}{M_\infty}$$

The turbulent eddy viscosity can be calculated from

$$\mu_T = c_\mu \frac{(\rho k)^2}{\rho\varepsilon}\frac{Re_\infty}{M_\infty}$$

$$c_\mu = 0.09\left(1 - e^{-0.0115y^+}\right)$$

$$y^+ = y_n\left[\frac{Re_\infty}{M_\infty}\frac{\rho|\nabla\times\bar{V}|}{\mu}\right]_{wall}^{1/2}$$

In the momentum equations μ is replaced with $\mu+\mu_T$ and in the energy equations, for the calculation of the heat flux, μ is replaced with $\mu+\mu_T \times Pr/Pr_T$ where *Pr* and Pr_T are laminar and turbulent Prandtl numbers. Pr = 0.75, Pr_T=0.9

$$Pr = 0.75; \quad Pr_T = 0.9$$

The production term for turbulence energy k can be calculated from

$$P = \left[\mu_T\left(2\frac{\partial u}{\partial x} - \phi\right)\frac{M_\infty}{Re_\infty} - \frac{2}{3}\rho k\right]\frac{\partial u}{\partial x} + \left[\mu_T\left(2\frac{\partial v}{\partial y} - \phi\right)\frac{M_\infty}{Re_\infty} - \frac{2}{3}\rho k\right]\frac{\partial v}{\partial y} + \mu_T\left(\frac{\partial u}{\partial y} + \frac{\partial v}{\partial x}\right)\frac{M_\infty}{Re_\infty}\left(\frac{\partial u}{\partial y} + \frac{\partial v}{\partial x}\right)$$

$$\phi = \frac{\partial u}{\partial x} + \frac{\partial v}{\partial y}$$

3.3 NUMERICAL SCHEME

The entire computational domain is discretized using finite volume discretization technique, which makes use of the integral equations of the flow variables. The values of the flow variables are calculated at the centroids of the finite volumes and their corresponding fluxes at cell faces.

The differential equations of the flow variables *U* are integrated over a finite volume V_i and after rearrangement of the terms, we obtain the following expression:

$$\Delta U_i = \Delta t \times Q_i + \frac{\Delta t}{V(i)} \times \left[S_{i-\frac{1}{2},j} \hat{F}_{i-\frac{1}{2},j} - S_{i+\frac{1}{2},j} \hat{F}_{i+\frac{1}{2},j} + S_{i,j-\frac{1}{2}} \hat{F}_{i,j-\frac{1}{2}} - S_{i,j+\frac{1}{2}} \hat{F}_{i,j+\frac{1}{2}} \right]$$

$$S_{i\pm\frac{1}{2},j} = \frac{1}{2}\left(S_{i,j} + S_{i\pm1,j}\right) S_{i,j\pm\frac{1}{2}} = \frac{1}{2}\left(S_{i,j} + S_{i,j\pm1}\right)$$

ΔU is calculated at every cell and an explicit integration has been achieved by adding the calculated ΔU to previous *U* value at cells and new values are updated. Δt used here is a local time step value specific to the cell.

Upwind differencing schemes are used in the calculation of the Flux terms. Upwind schemes use the velocity and direction of propagation of the flow information, hence ensuring better results. To ensure better resolution of the shocks and to get better numerical accuracy flux vector splitting is employed. Van Leer flux vector splitting has been used to split the inviscid flux terms into a positive and negative part based on their characteristic speeds. Van Leer flux vector splitting allows a continuous flux vector splitting across supersonic (positive and negative directions) and subsonic flow regimes and thus ensuring a smooth transition in the flow parameters during calculation.(a is characteristic velocity in the following.)

$$\hat{F}_{i+\frac{1}{2},j} = \hat{F}^{+} U^{-}_{i+\frac{1}{2},j} + \hat{F}^{-} U^{+}_{i+\frac{1}{2},j}$$

$$F^{\pm} = \begin{bmatrix} f^{\pm} \\ f^{\pm}((\gamma-1)/u \pm 2a) \\ f^{\pm}v \\ f^{\pm}(E+p)/\rho \\ f^{\pm}(\rho k)/\rho \\ f^{\pm}(\rho\varepsilon)/\rho \end{bmatrix}$$

$$f^{\pm} = \rho c\left[\frac{1}{2}(M_x \pm 1)\right]^2$$

U^+ and U^- can be chosen depending on the degree of up-winding needed, - 1st,2nd order up-winding, or 2nd,3rd order upwind biased, or 2nd order central differencing (See Ref.[1]).

Thin layer approximation is used in the calculation of the viscous fluxes. It is assumed that the derivatives of the flow variables are dominant in the stream wise direction as compared to that of the cross stream direction. The normal derivatives are hence neglected. The eqns. for viscous fluxes for *k* and ε are

$$\hat{F}_{k_{i+1/2,j}} = -\frac{M_\infty}{Re_\infty}\frac{1}{d_{i+\frac{1}{2},j}}\frac{1}{2}\left[\mu_{i+1,j} + \mu_{i,j} + \frac{1}{\sigma_k}\left(\mu_{T_{i+1,j}} + \mu_{T_{i,j}}\right)\right]\left[k_{i+1,j} - k_{i,j}\right]$$

$$\hat{F}_{\varepsilon_{i+1/2,j}} = -\frac{M_\infty}{Re_\infty}\frac{1}{d_{i+\frac{1}{2},j}}\frac{1}{2}\left[\mu_{i+1,j} + \mu_{i,j} + \frac{1}{\sigma_\varepsilon}\left(\mu_{T_{i+1,j}} + \mu_{T_{i,j}}\right)\right]\left[\varepsilon_{i+1,j} - \varepsilon_{i,j}\right]$$

The viscous fluxes of x-direction momentum and energy equations are modified to

$$\hat{F}_{2_{i+1/2,j}} = -\frac{M_\infty}{Re_\infty}\frac{1}{d_{i+\frac{1}{2},j}}\left[\left(u_{i+1,j} - u_{i,j}\right) + \frac{n_{x_{i+\frac{1}{2}}}}{3}\left(\bar{u}_{i+1,j} - \bar{u}_{i,j}\right)\right] + \frac{1}{3}\left[(\rho k)_{i+1} + (\rho k)_i\right]$$

$$\hat{F}_{4_{i+1/2,j}} = u_{i+\frac{1}{2},j}\hat{F}_{2_{i+1/2,j}} + v_{i+\frac{1}{2},j}\hat{F}_{3_{i+1/2,j}} - \frac{M_\infty \mu}{Re_\infty Pr(\gamma-1)}(T_{i+1} - T_i)$$

$$+\frac{1}{3}\left[(\rho k)_{i+1}u_{i+1} + (\rho k)_i u_i\right]$$

The fluxes at remaining faces of the cell can be calculated in the same manner.

3.4 BOUNDARY AND INITIAL CONDITIONS

At the solid wall, the values of k and ε are taken left free. At the inlet the values of k and ε are taken as free stream values. At the free stream their values are left free. The viscous fluxes of k and ε are taken to be zero at the solid wall. Flux vector splitting is not used at the solid boundary.

The initial values of both the k and ε are taken as 1E-05 and eddy viscosity coefficient is taken as 0. The order of discretization (central or upwind), and the *CFL* number are varied after certain iterations to increase the accuracy of the solution and to accelerate the convergence.

4. VALIDATION OF IMPLEMENTED TURBULENCE MODELS

An attempt was made to validate the implemented turbulence models for two test cases: supersonic flow over a flat plate, and transonic flow over an axisymmetric bump. Spallart-Allmaras (S-A) which was already implemented in the solver is validated here.

4.1 FLAT PLATE

4.1.1 Problem formulation:

Supersonic flow over a flat plate at zero AOA was simulated using the implemented turbulence models. The simulations were performed for a flat plate of length 0.5 meters. The origin was chosen at the leading edge for the simulations. The grid used was generated using FORTRAN program. A second order accurate upwind scheme was used for simulating the flow over the flat plate. The reference conditions used are as follows:

MACH NO.	2.27
STATIC PRESSURE (Pa)	17336.87
STATIC TEMPERATURE (k)	158.05
WALL TEMPERATURE (k)	344.5

Table 1: Reference conditions used for simulating supersonic flow over a flat plate

4.1.2 Grid independence and domain:

Grid independence was performed for all the turbulence models. The domain length was chosen to be 0.8m in Y-direction so the there is no reflection of shock happening at the top boundary. The domain length 0.8m proved to be more than sufficient for the required purpose see Figure1, so domain length can be reduced in y-direction for saving the computation time; this endeavor was not pursued for the following simulations. The grid sizes used for grid independence were 100*100 and 150*150 respectively in X and Y direction. Variation of skin friction coefficient Cf along the flat plate was compared to ensure grid independence. The following are the grid used; grid independence plots and pressure palette obtained using Baldwin Lomax showing the leading edge shock capture. In the grid used the normal distance of the first cell from the wall are $2\mu m$.

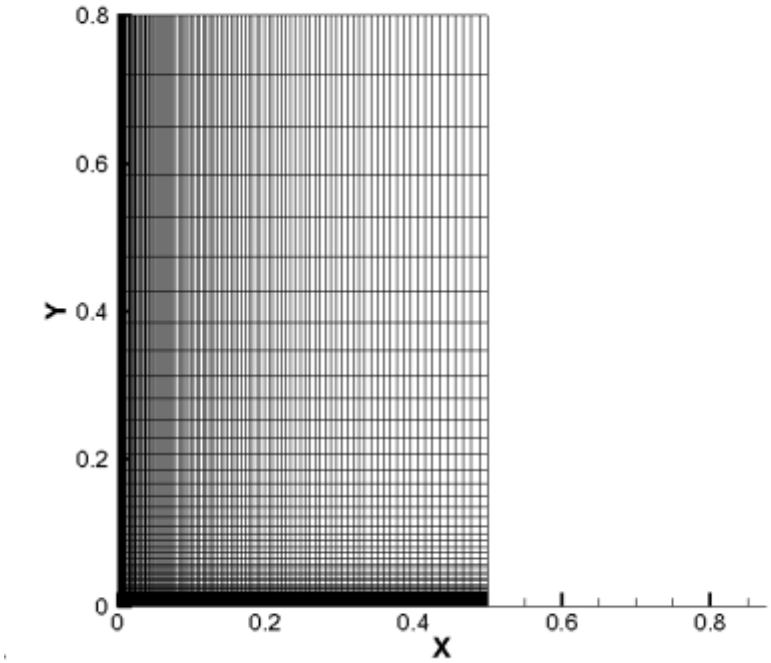

Figure 1: flat plate grid 100*100

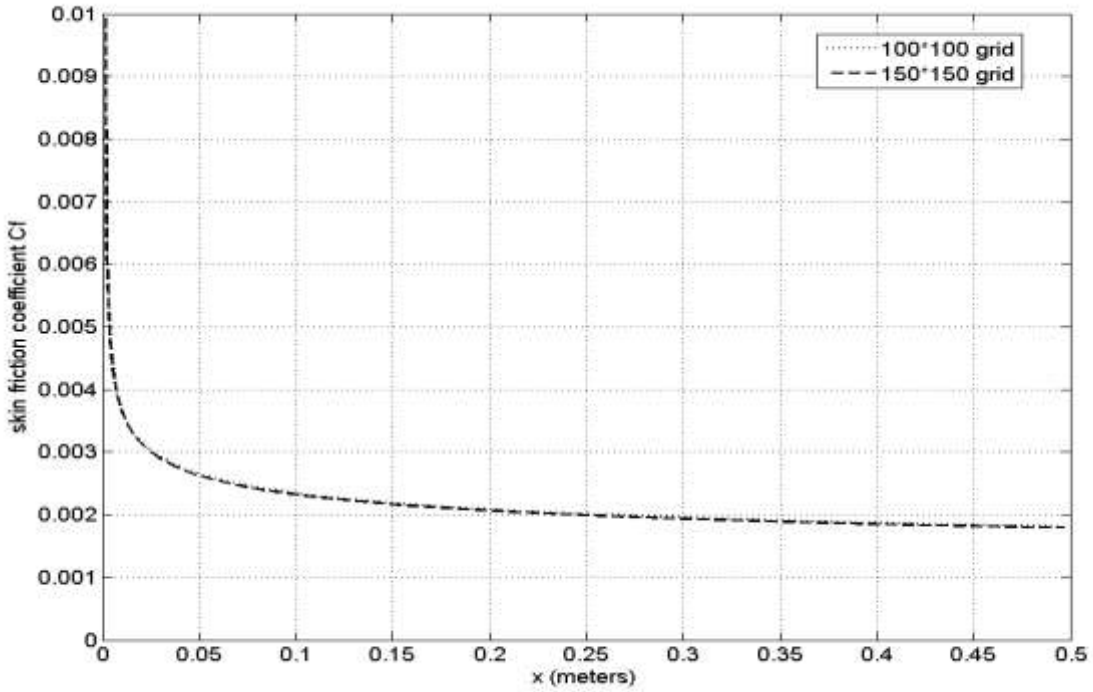

Figure 2: flat plate grid independence for Johnson-king model

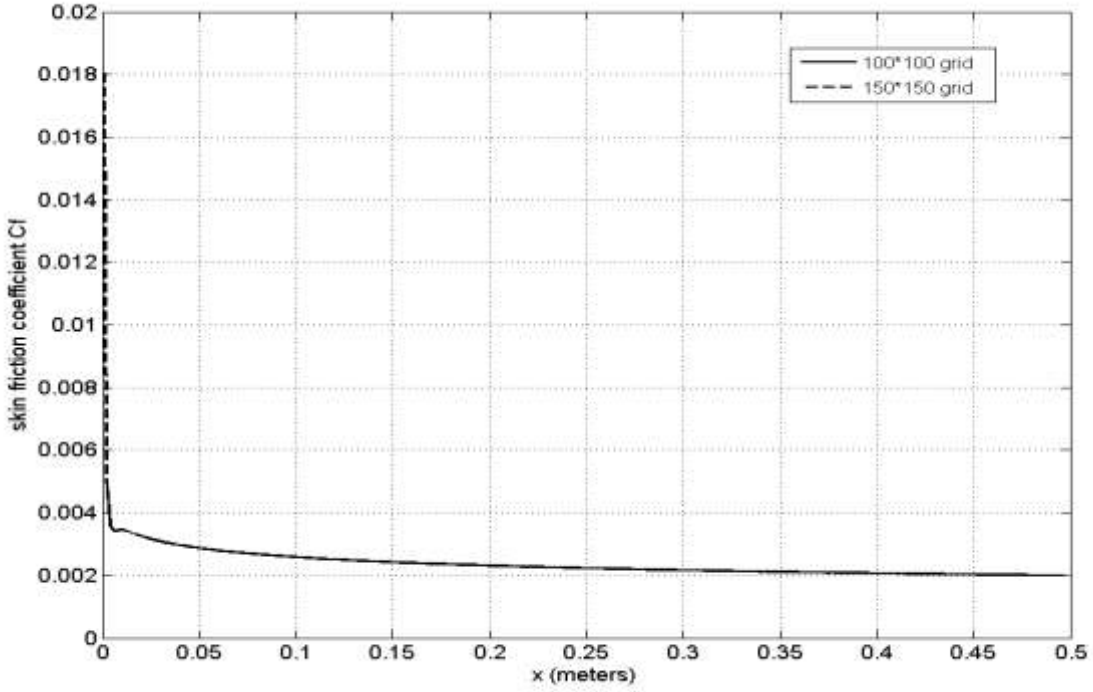

Figure 3: flat plate grid independence for S-A model

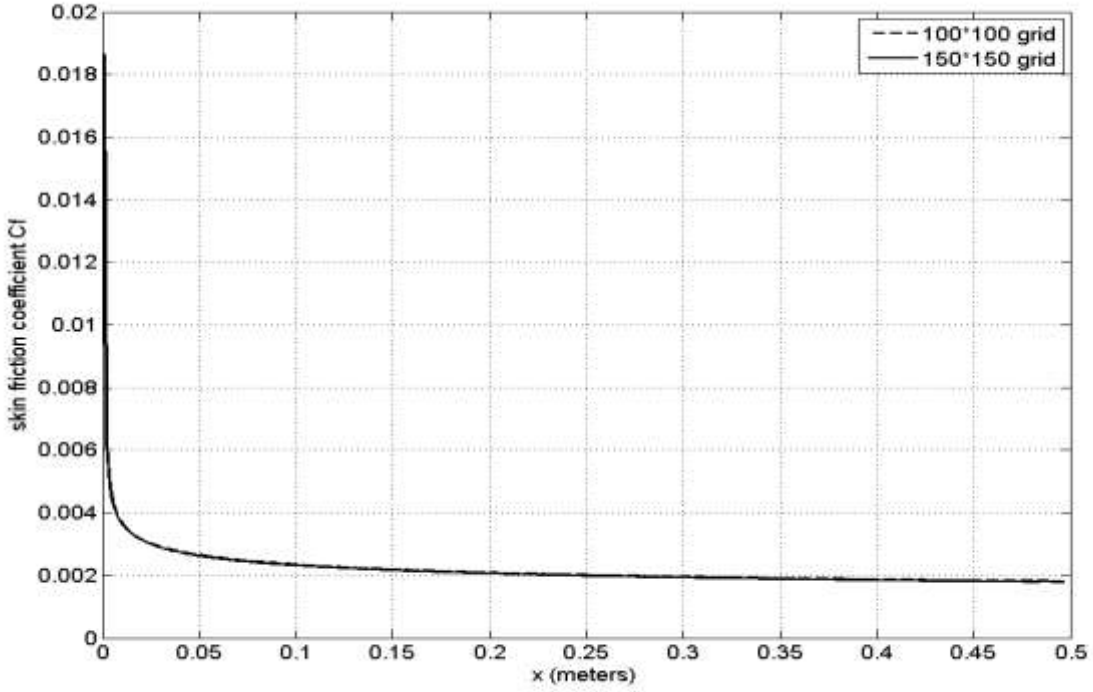

Figure 4: flat plate grid independence for modified Johnson-king model

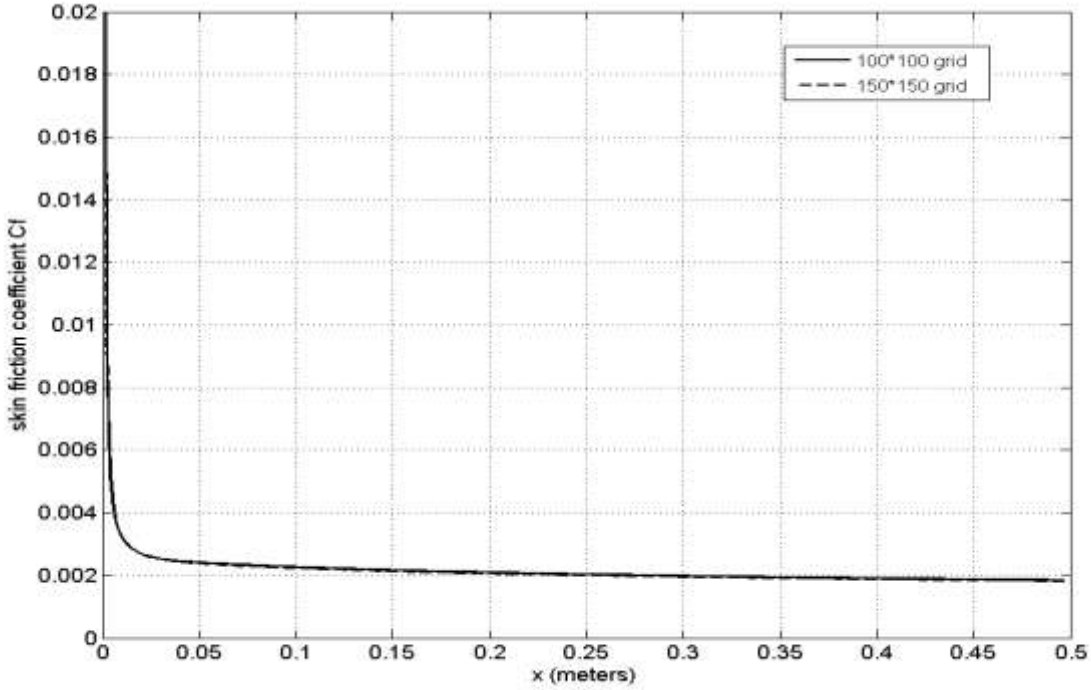

Figure 5: flat plate grid independence for chein's k-epsilon model

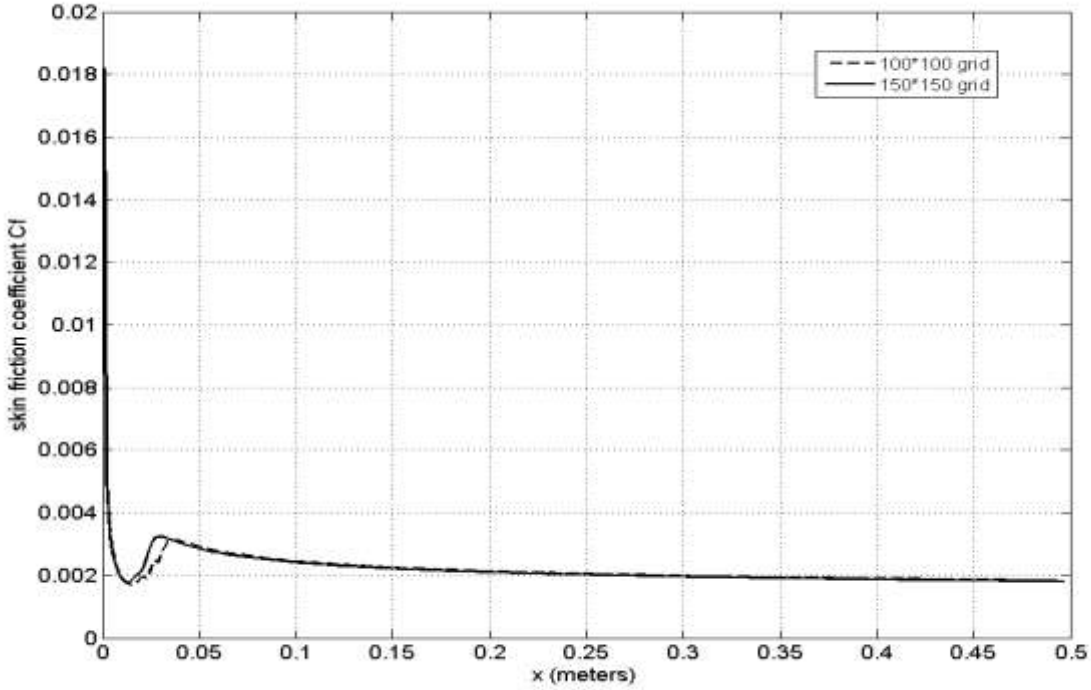

Figure 6: variation of Cf along X for different grids using Baldwin Lomax for flat plate

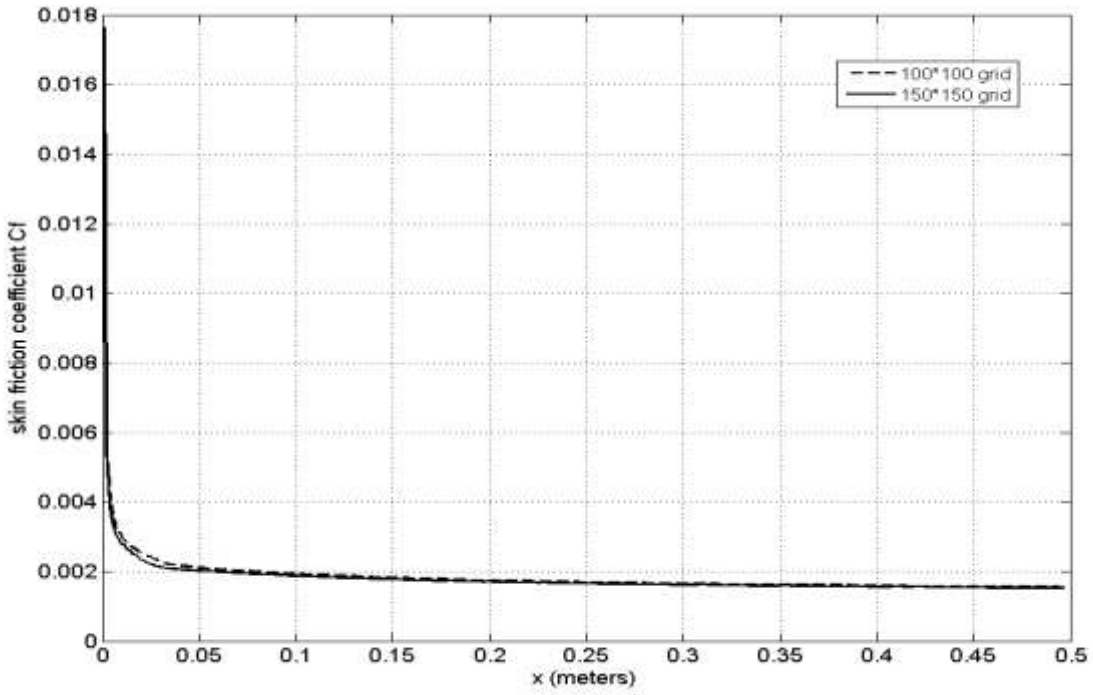

Figure 7: variation of Cf along X for different grids using Johnson-Abid model for flat plate

Grid independence could be achieved using 100*100 and 150*150 grid for most of turbulence models, except for Baldwin Lomax and Johnson Abid model as shown in above Figures 3 to 8. In the data compared with experimental results solutions corresponding to 100*100 grids are presented.

4.1.3 Results:

Flow field: Due to the viscosity of the fluid a boundary layer starts to develop at the leading edge of the flat plate. The oncoming free stream experiences a displacement effect, because the boundary layer on the flat plate posses a fictitious curvature resulting in the formation of leading edge shock wave as show in the following pressure pallets. Following are the plots showing the comparison of simulation results to that of experimental results from Ref. [7].

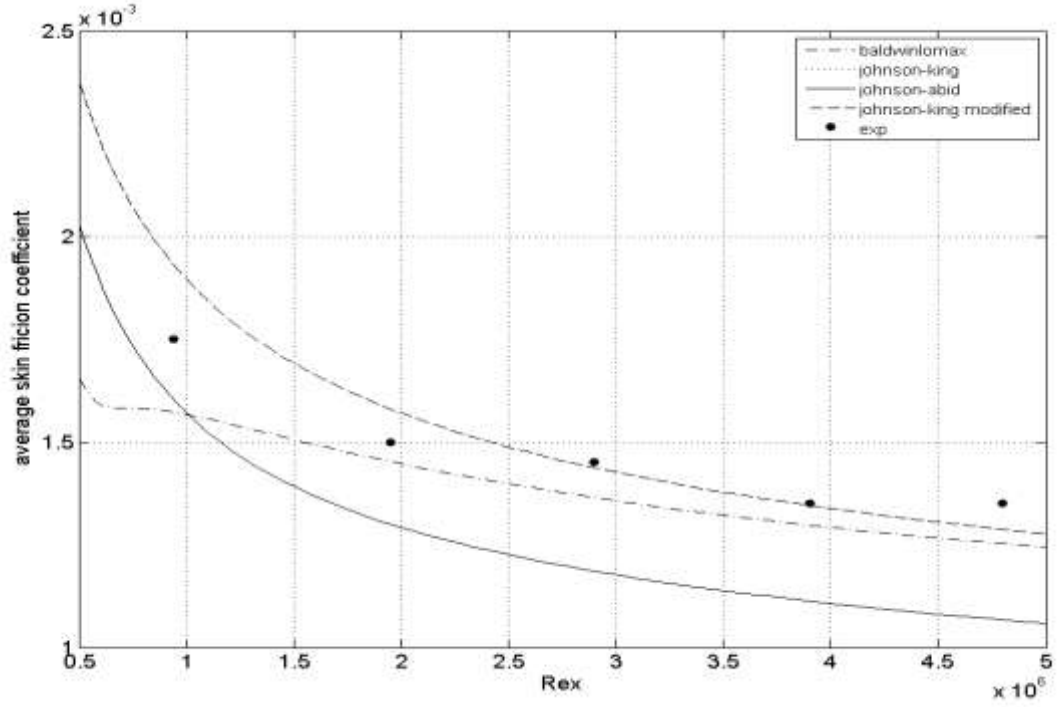

Figure 8: comparison of average skin friction on flat plate from simulation with experimental results for algebraic models

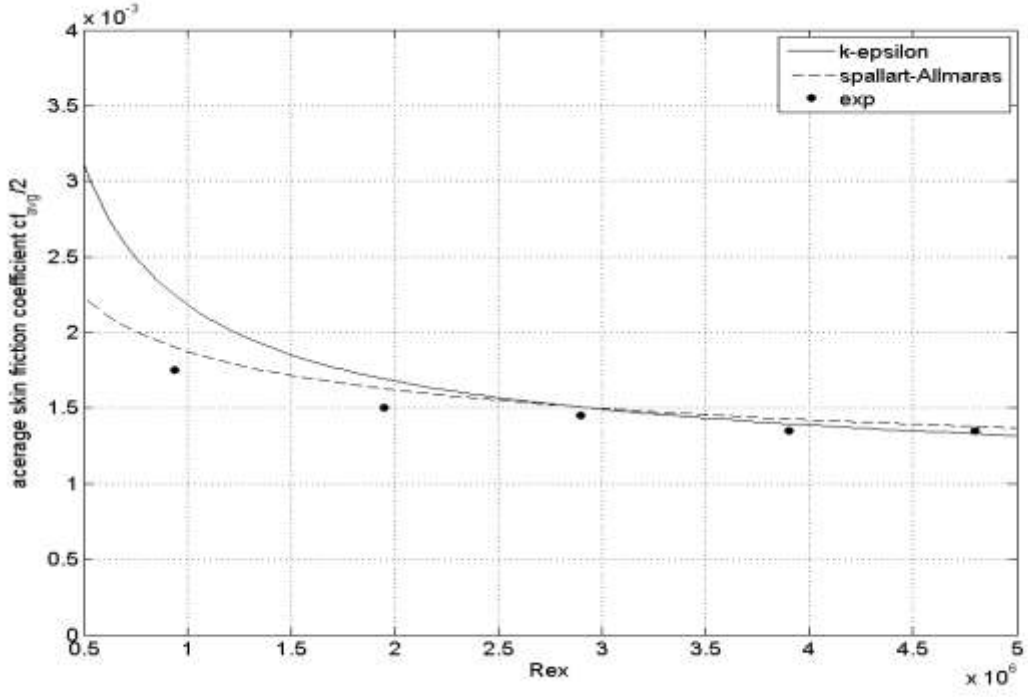

Figure 9 comparison of average skin friction on flat plate from simulation with experimental for S-A and K-epsilon model

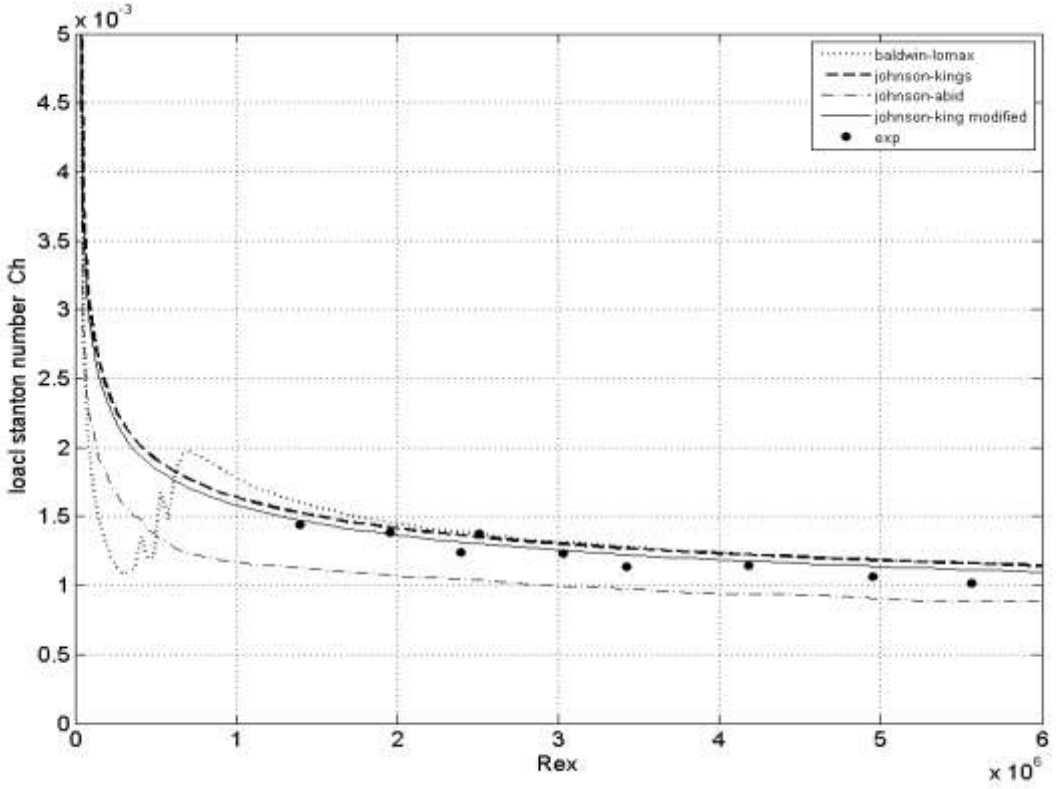

Figure 10: comparison of local Stanton number on a flat plate from simulation with experimental results for algebraic models

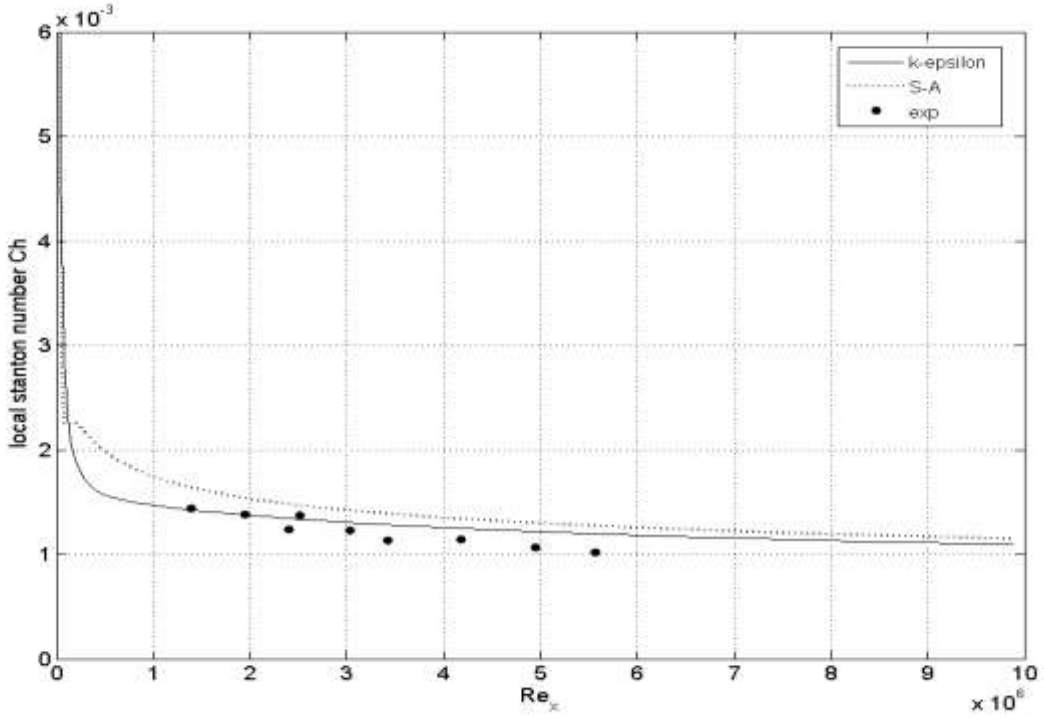

Figure 11: comparison of local Stanton number on flat plate from simulation with experimental for S-A and chein's K-epsilon models

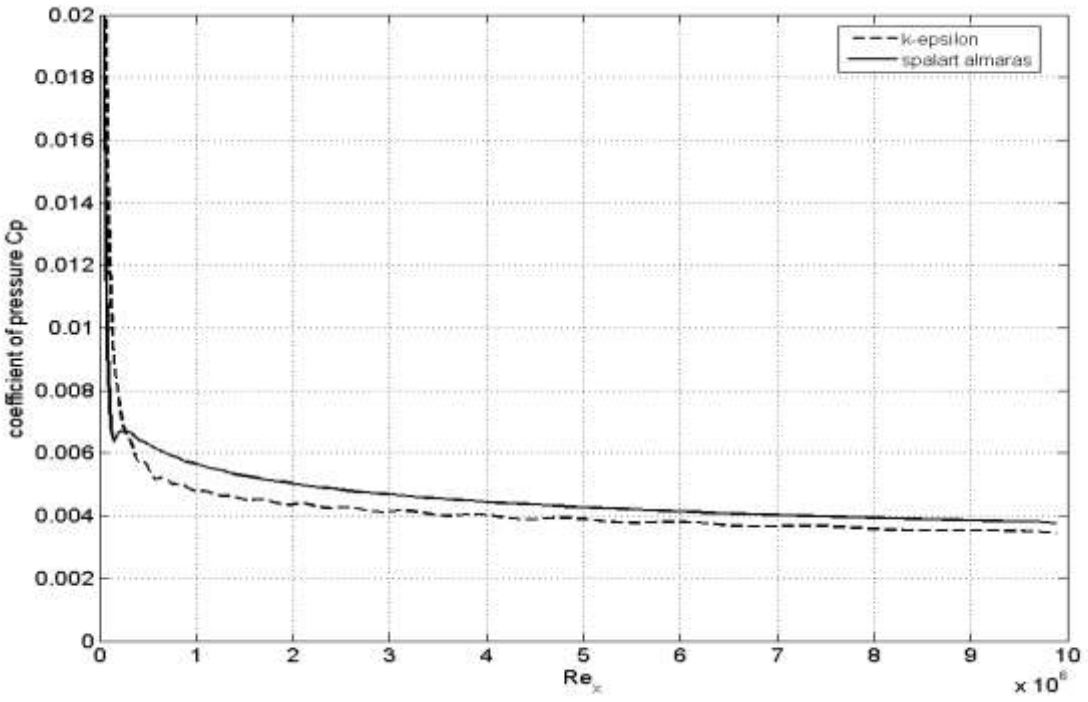

Figure 12: variation of Cp along the plate using S-A and cheins k-epsilon model for a flat plate

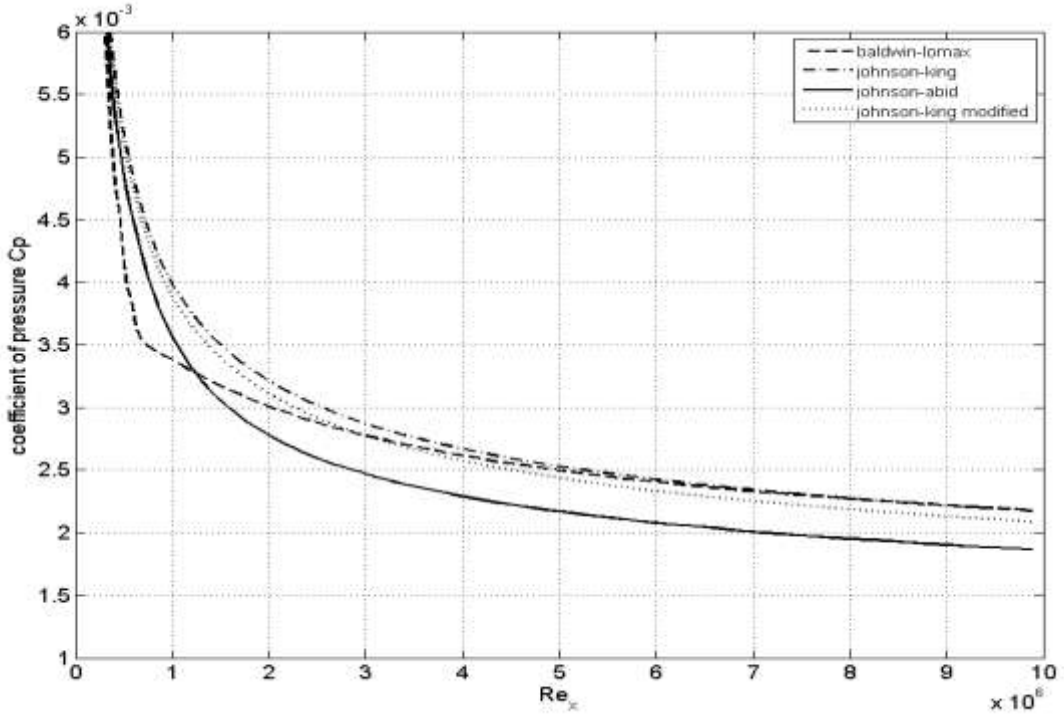

Figure 13: variation of Cp along the body for algebraic models for flat plate

The comparison of average skin friction and Stanton number of Johnson- Abid model with experimental results is not as good as Johnson-king model. The most probable reason for this behavior would have been the use of approximate estimates for boundary layer thickness and boundary layer edge velocity in this model. There is no improvement in the result for modified Johnson-king model compared to Johnson–king model. The K-Epsilon model is also found to give good results for the flat plate simulation. The results for Stanton No. predicted by k-ε are found to be closer to the solution than S-A. It is also observed during the simulations that k-ε is very sensitive to numerical perturbations. The initial value of the turbulent energy and dissipation rate has to carefully chosen. Incorrect initial values of the parameters have a tendency to diverge the solution. Initial iterations of the solver are run for laminar model, and subsequently turbulence model is turned on. This exercise makes the subsequent iterations more stable.

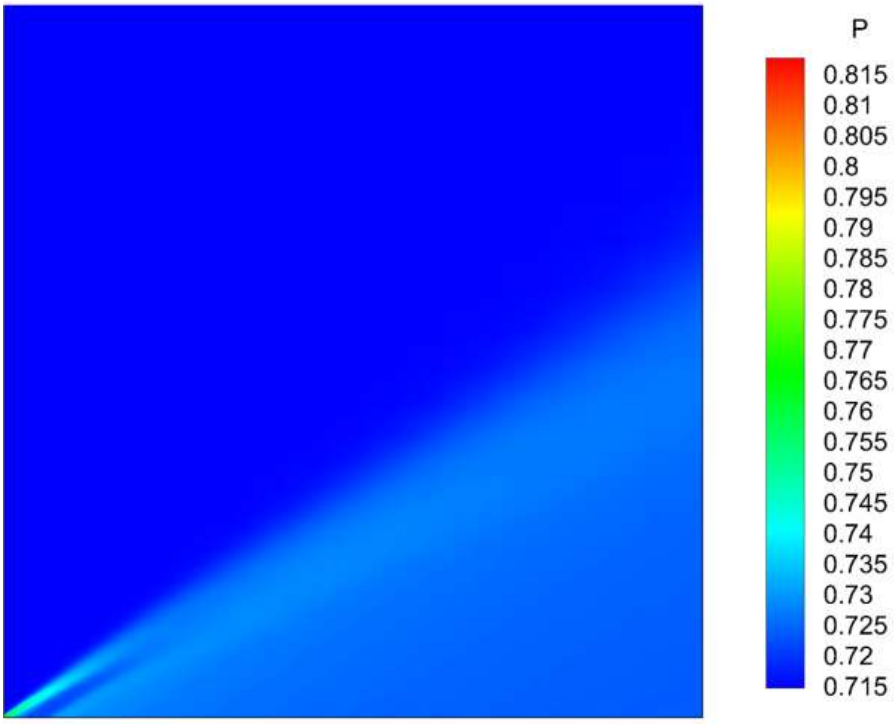

Figure 14: pressure contours obtained over flat plate using Baldwin Lomax model

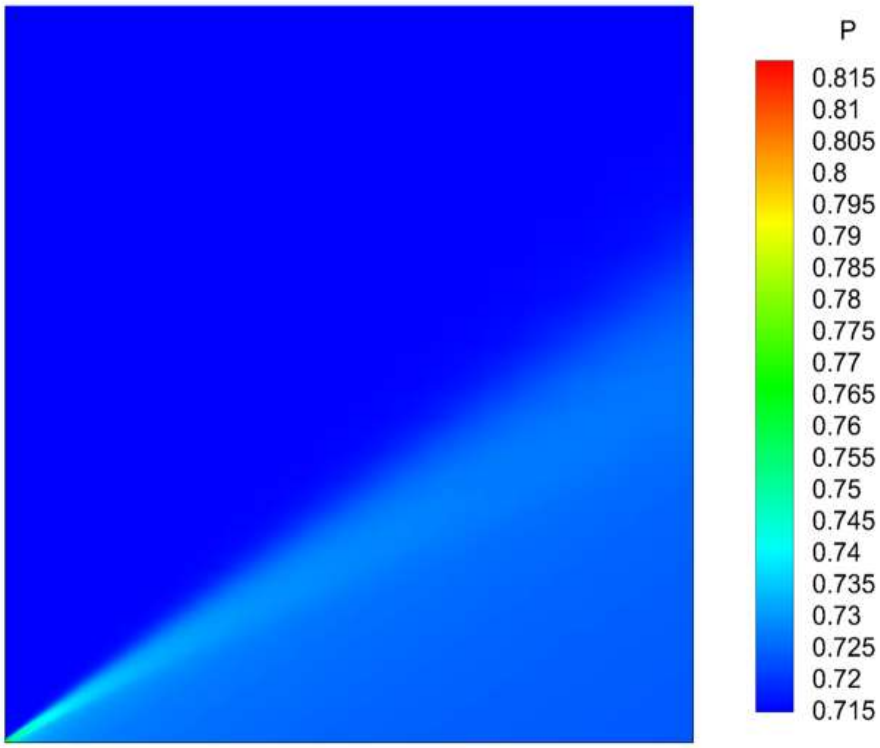

Figure 15: pressure contours obtained over flatplate using Johnson-king model

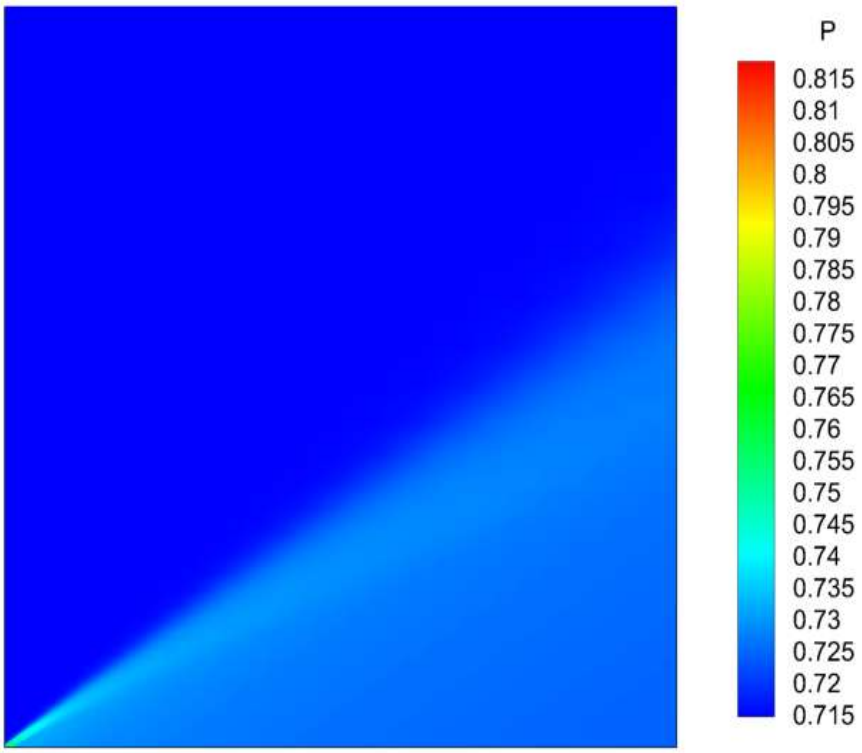

Figure 16: pressure contours obtained over flatplate using S-A model

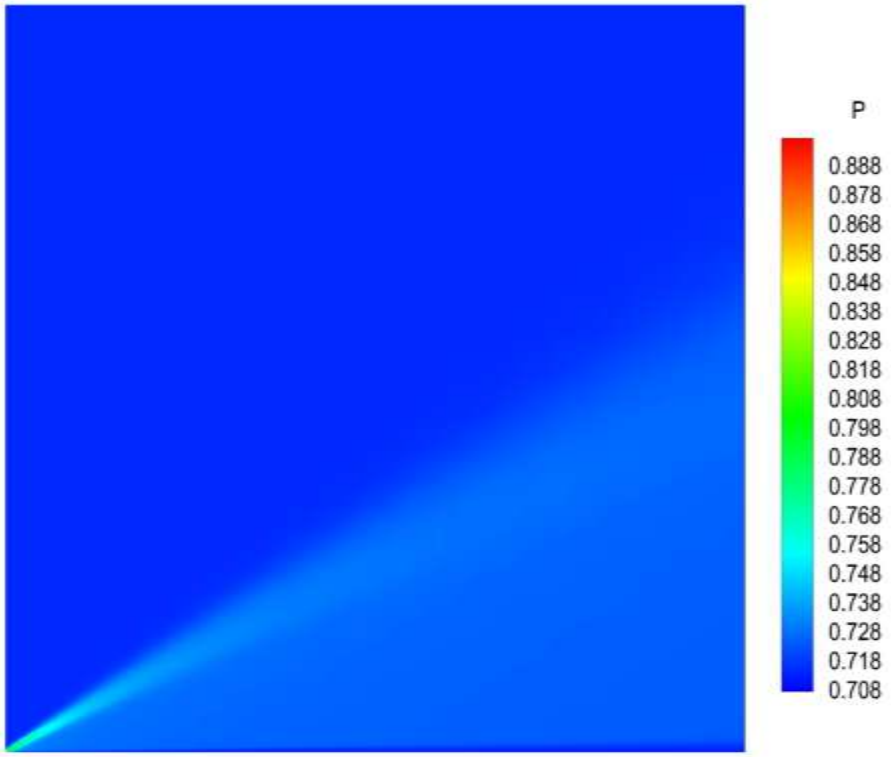

Figure 17: pressure contours obtained over flat plate using chein's k-epsilon model

Following table shows the Cd predicted by different models.

Model	Baldwin-Lomax	Johnson-king	Modified Johnson-king	Johnson-Abid	Spallart-Allmaras	Chiens k-ε model
C_D predicted	0.00109	0.001105	0.0010587	0.00092601	0.001199	0.001148

Table 2: comparison of Cd predicted by different models for supersonic flow over a flatplate

In comparison of Figures 14 to 17 it can be seen that shock capturer is reasonably good in all the models except Baldwin Lomax. In the Figures 3 and 6 it can be seen that there is a kink near the leading edge for local Stanton number and skin friction coefficient when Baldwin Lomax and Spallart-Allamaras models were used. This might be because of the way these two models capture leading edge compared to other models see pressure contours for different models. All the Johnson-king model variants predicted similar pressure contours.

4.2 AXISYMMETRIC BUMP

4.2.1 Problem formulation:

Transonic flow over an axisymmetric bump was simulated with turbulence being predicted by the implemented models. The geometry used is as shown in the Figure 18. The grid was generated using a FORTRAN program. A third order accurate upwind scheme is used for simulating transonic flow over the bump. The origin was chosen to be at the leading edge of the bump. Following are the reference conditions used in the simulations:

MACH NO.	0.875
REYNOLDS NUMBER	2.761e06
STATIC PRESSURE (Pa)	101956
STATIC TEMPERATURE (K)	288

Table 3: reference conditions used for simulating transonic flow over a circular arc bump

4.2.2 Grid independence and domain:

Grid independence was performed for all the turbulence models. The domain chosen for simulation is shown in the following Figure 19. The domain was sufficiently large to accommodate the shock formed on the bump. The grid was non-dimensionalized with the cord length of the circular arc bump. In the grid used the normal distance of the first cell from the wall is $1\mu m$. Following table shows the grids used for grid independence.

	No .of grid points upwind of the bump	No .of grid points on the bump	No. of grid points downwind of bump	No. of grid points in cross stream direction
180*100	60	60	60	100
180*140	60	60	60	140
270*180	90	90	90	180
360*180	120	120	120	180

Table 4: sizes of grids used for circular arc bump

.

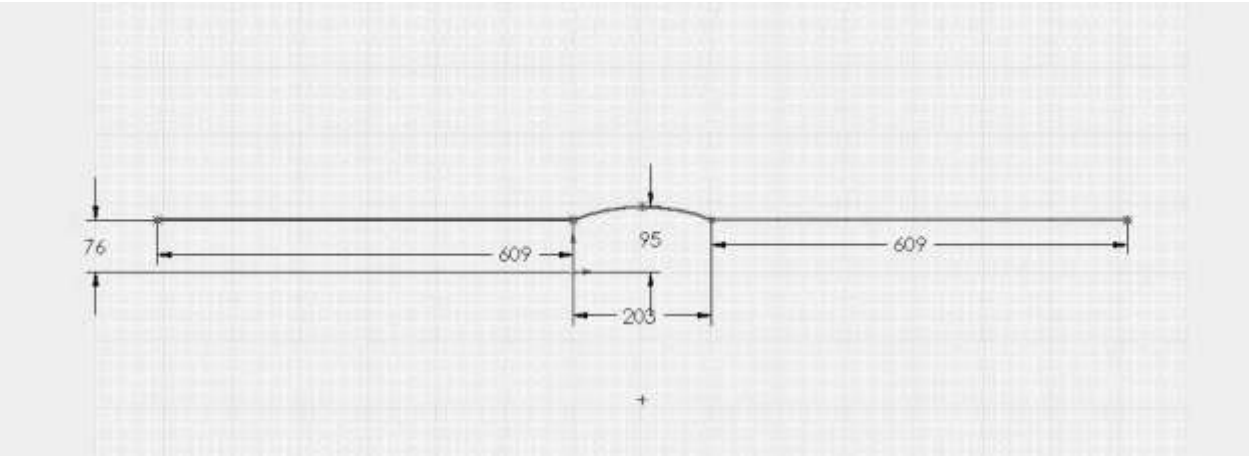

Figure 18: geometry of circular arc bump

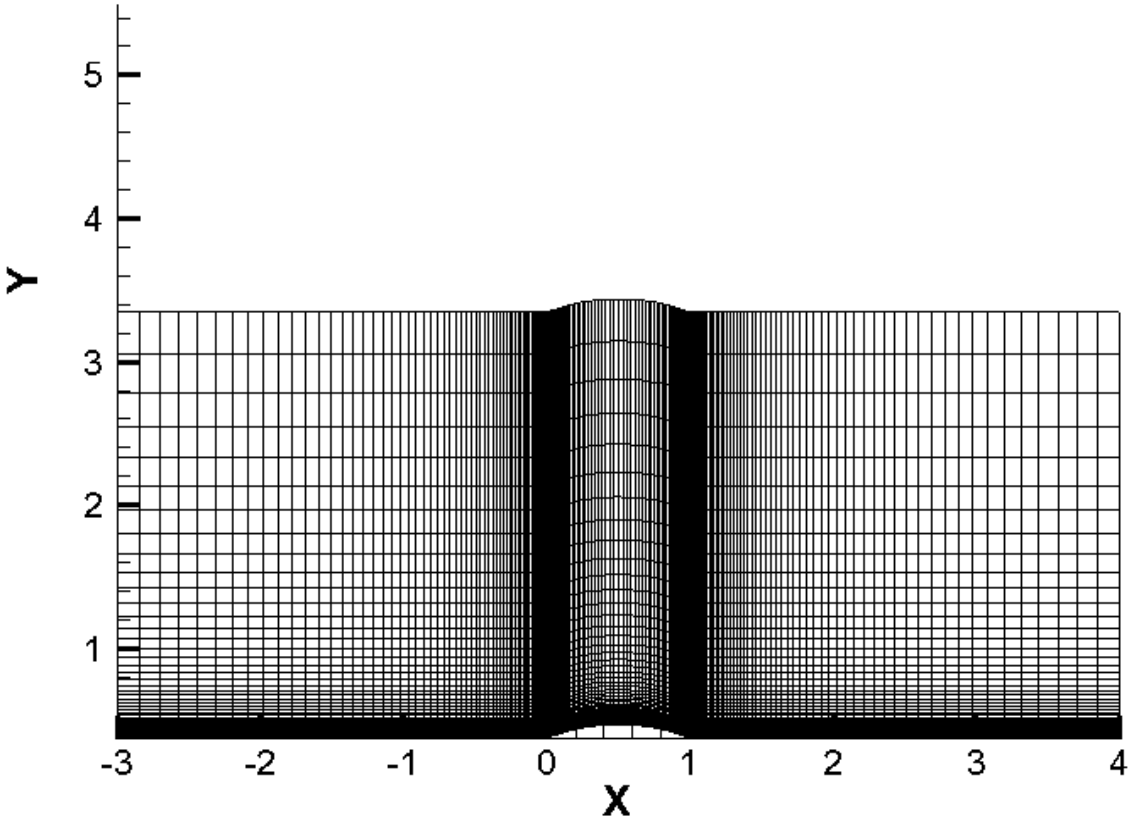

Figure 19: grid used for axisymmetric bump

Grid independence study was done only for S-A and Baldwin Lomax model, due to lack of time. For rest of the models solution for grid 180*140 is used for comparison with experimental results which are reasonably good. Skin friction coefficient along the bump was

compared for grid independence studies. The following are the plots showing grid independence for Baldwin-Lomax and S-A model.

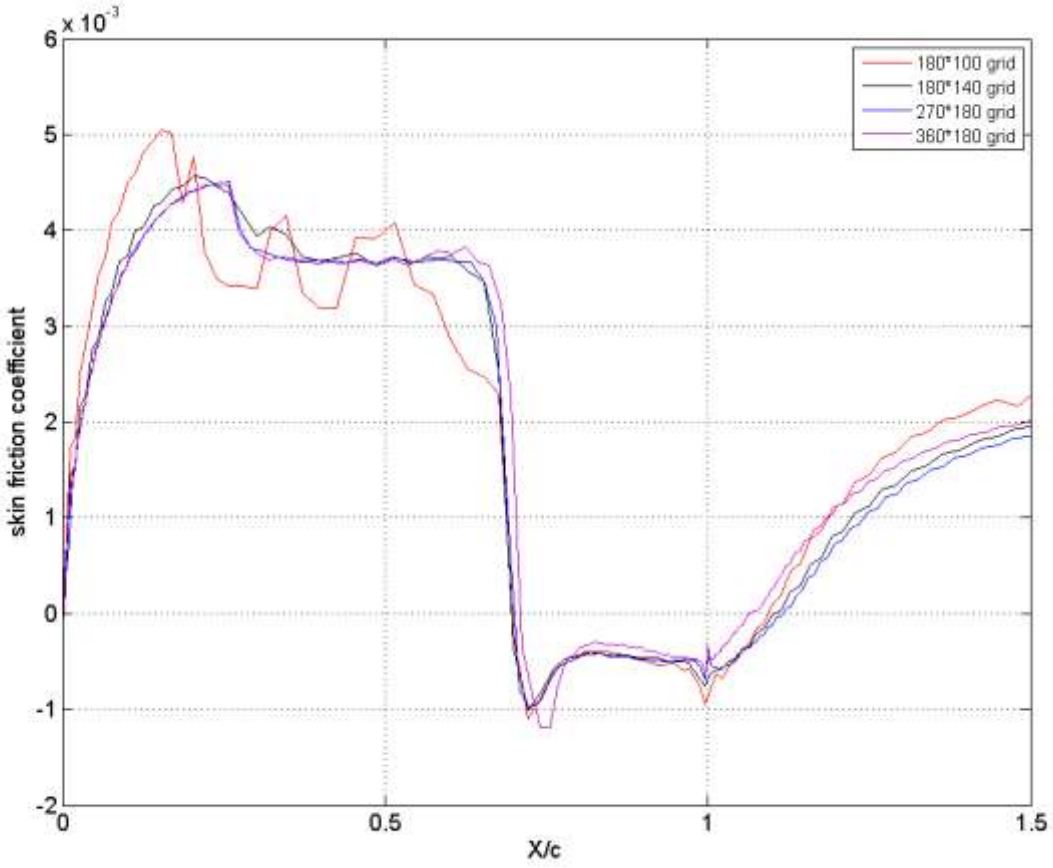

Figure 20: variation of Cf for different grids using BaldwinLomax model.

For Baldwin Lomax model grid independence could not be achieved with the above grids, because of its inability to predict flow separation and non-equilibrium characteristic properly. For S-A model grids 270*180 and 360*180 were giving same solutions, shown in the following figure. For Baldwin-Lomax and S-A model solution was presented for grid 270*180.

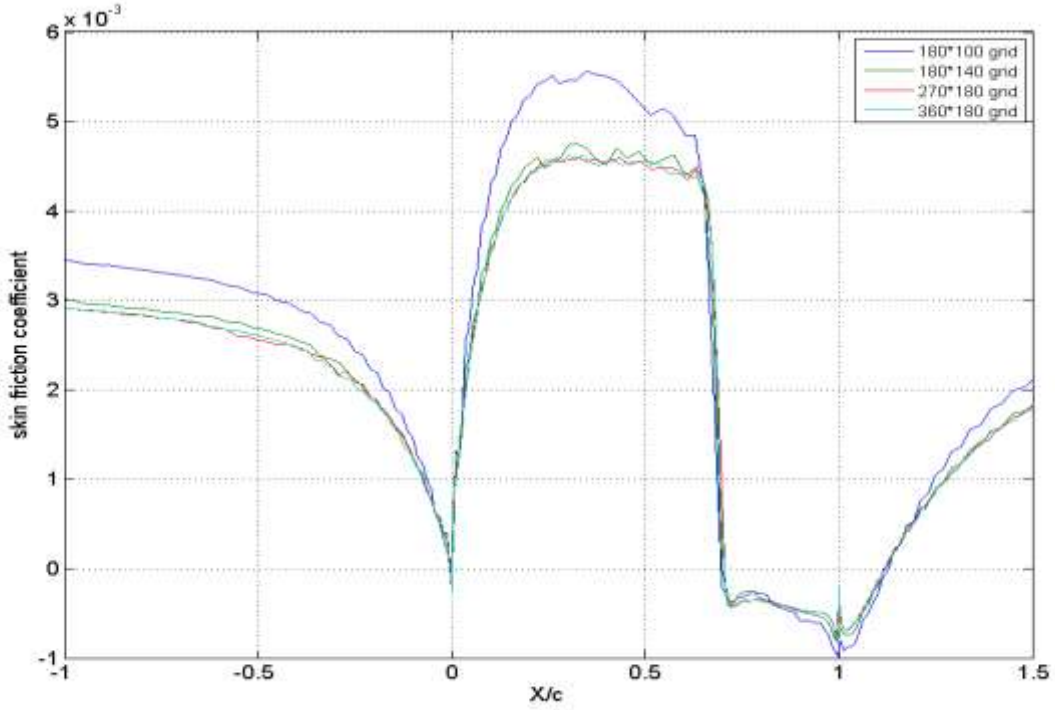

Figure 21: variation of skin friction along the bump using S-A model

4.2.3 Results obtained from algebraic and S-A model:

Flow field: Important characteristics of transonic turbulent boundary flow on the circular are bump are the normal shock wave on the circular arc and flow separation following the shock wave. A normal shock wave forms on the circular arc bump because of the acceleration that flow undergoes as it passes over the bump. Flow separation happens because of the adverse pressure gradient over the bump acting on the accelerated flow, which is also aided by the adverse pressure gradient created by the shock wave within the boundary layer. Following are the plots showing the comparison of simulation data to that of experimental data (from Ref. [8]) for Baldwin-Lomax, Johnson-king, modified Johnson-king, Johnson-Abid and S-A model.

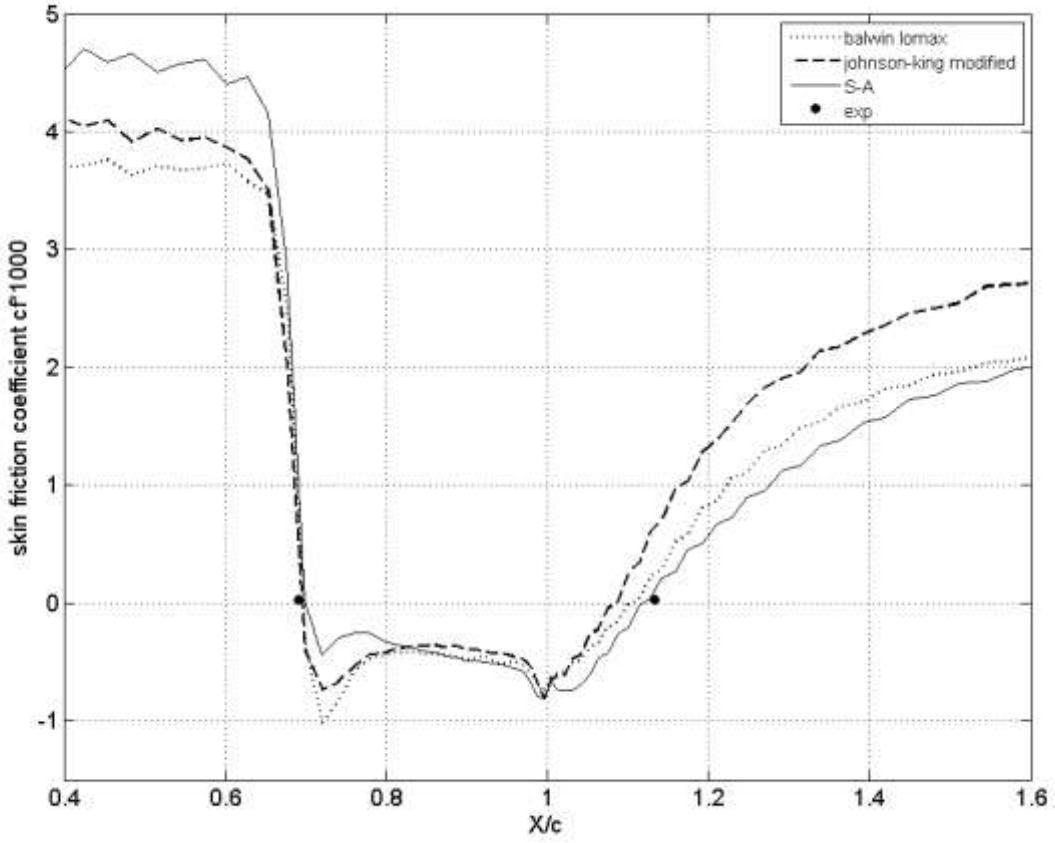

Figure 22: comparison of separation and attachment point for Baldwin-Lomax, S-A and Johnson-king models with experimental data

From the above a plot it can be observed that the skin friction values predicted by S-A, Baldwin–Lomax, and Johnson–king are very different at most of the points, especially before the shock and after the reattachment point. S-A predicts a higher skin friction before the shock compared to other two models. The separation points for all the three models is same, but Baldwin Lomax is predicting a bigger separation bubble compared to that of S-A. Johnson-kings model predicts flow reattachment to happen ahead compared to other models, as expected of it. Johnson-kings model tends to over predict the skin friction after reattachment point. So modifications were done to improve the solution.

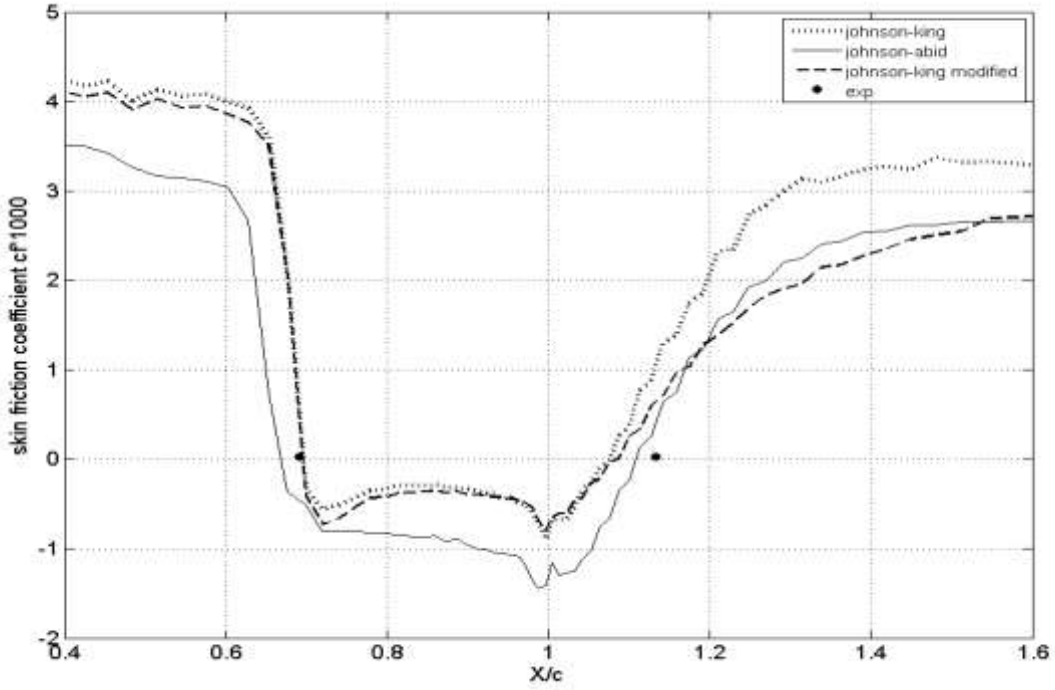

Figure 23: comparision of seperation and attachment point for different versions of Johnson and Kings model with experimental data

From the above plot modified Johnson-kings model is predicting much better value for skin friction (i.e., which are similar to S-A model) compared to Johnson-king model. The Johnson- Abid model even though is predicting a much better reattachment point, it is showing a larger separation bubble and predicting very less skin friction values compared to other models unwind of the shock wave. Following plots show the comparison of coefficient of pressure Cp and velocity profiles predicted by different models with experimental results. The computation results are in good comparison with the experimental results. In the figures 24 to 28 a comparison of Cp with experimental results is done. It is observed that Johnson-Abid model gives better values of Cp over the bump when compared to other models.

Model	Baldwin-Lomax	Johnson-king	Modified Johnson-king	Johnson-Abid	Spallart-Allmaras
C_D predicted	0.107031	0.1148	0.111497	0.1125	0.109573

Table 5: comparison of Cd predicted by different models for transonic flow over the bump

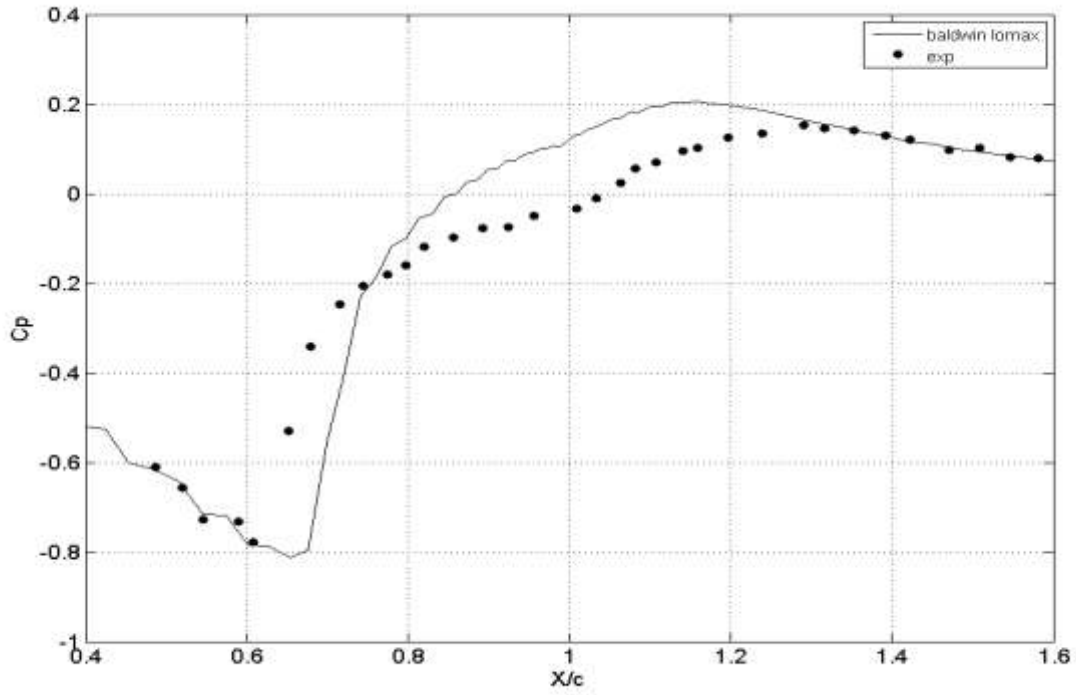

Figure 24:cp comparison with experimental data Baldwin-Lomax model

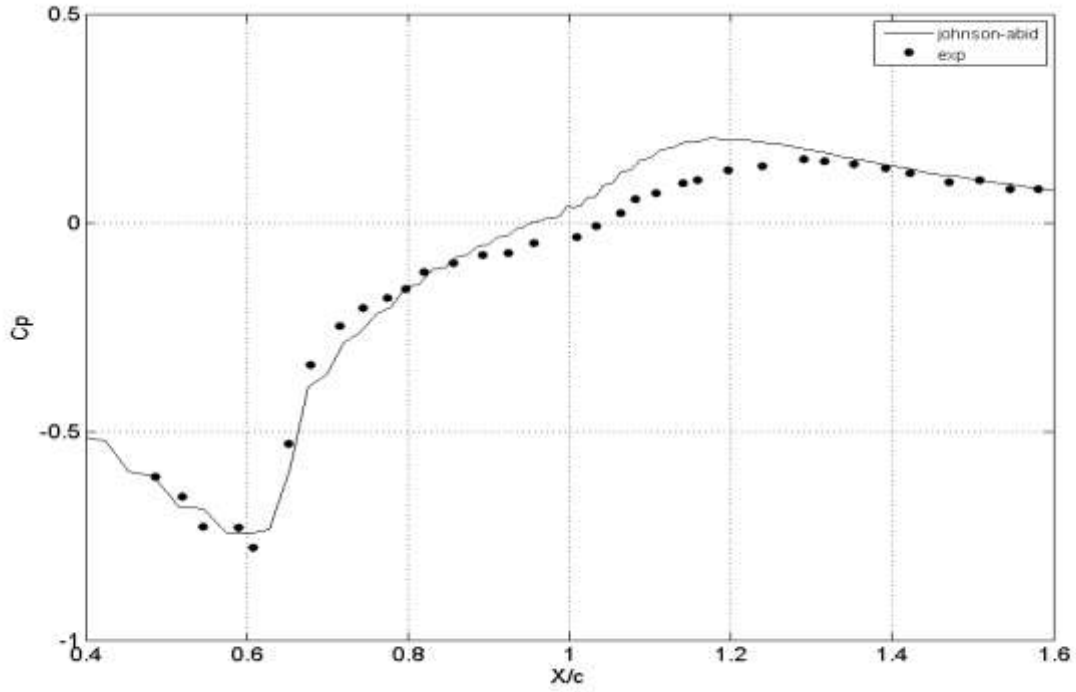

Figure 25: cp comparison with experimental data Johnson-Abid model

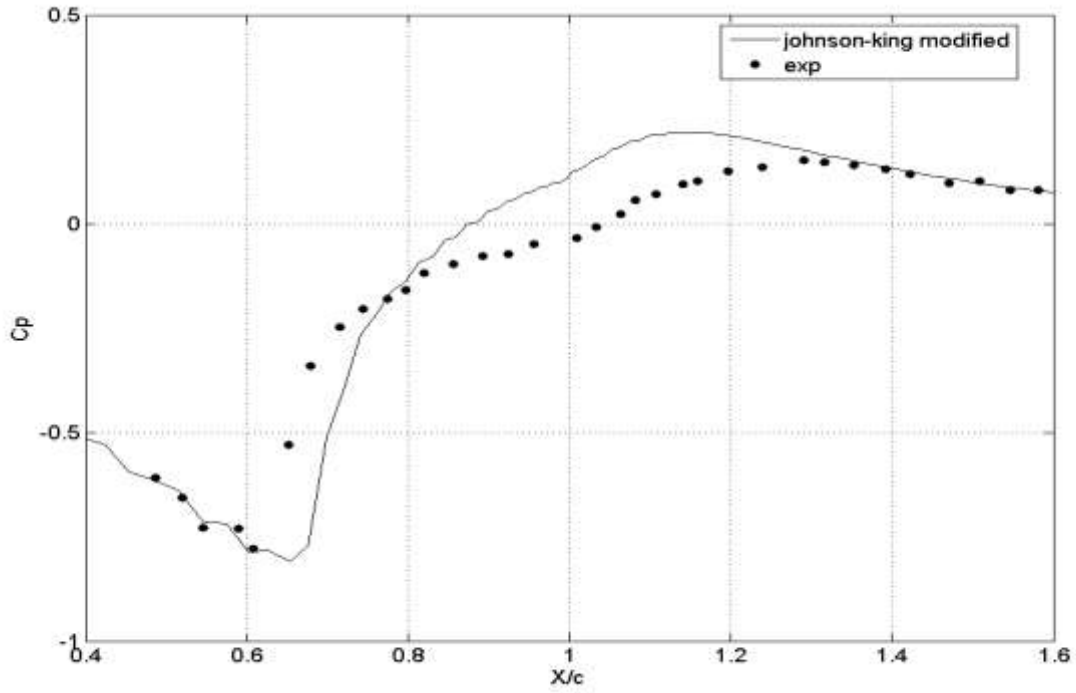

Figure 26:cp comparison with experimental data Johnson-king modified model

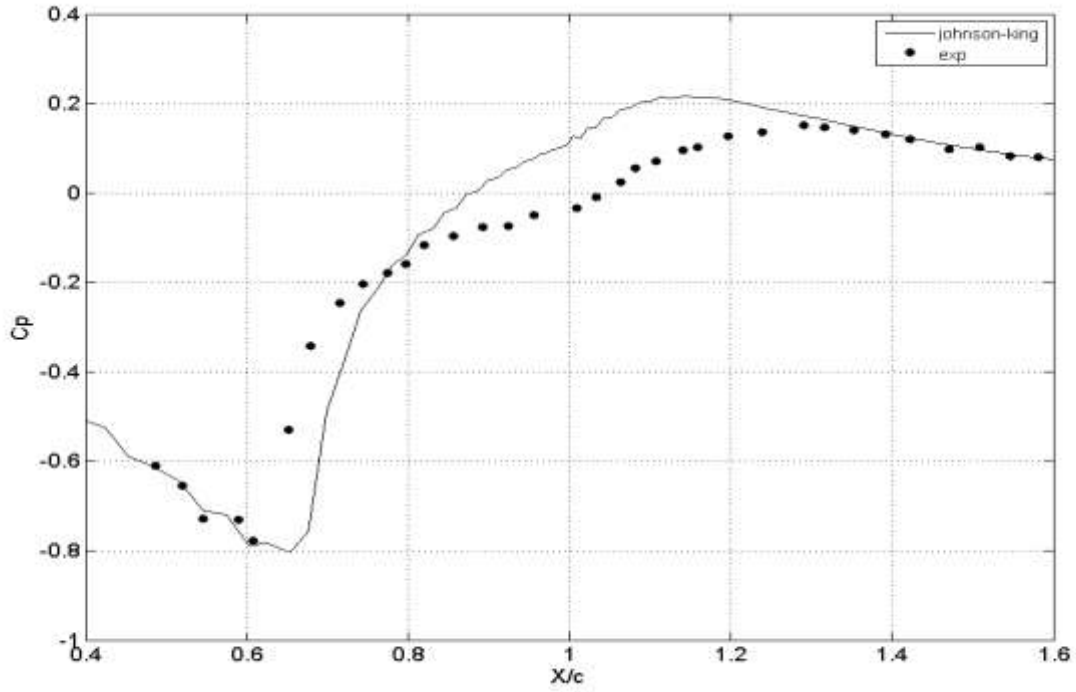

Figure 27: cp comparison with experimental data Johnson-king model

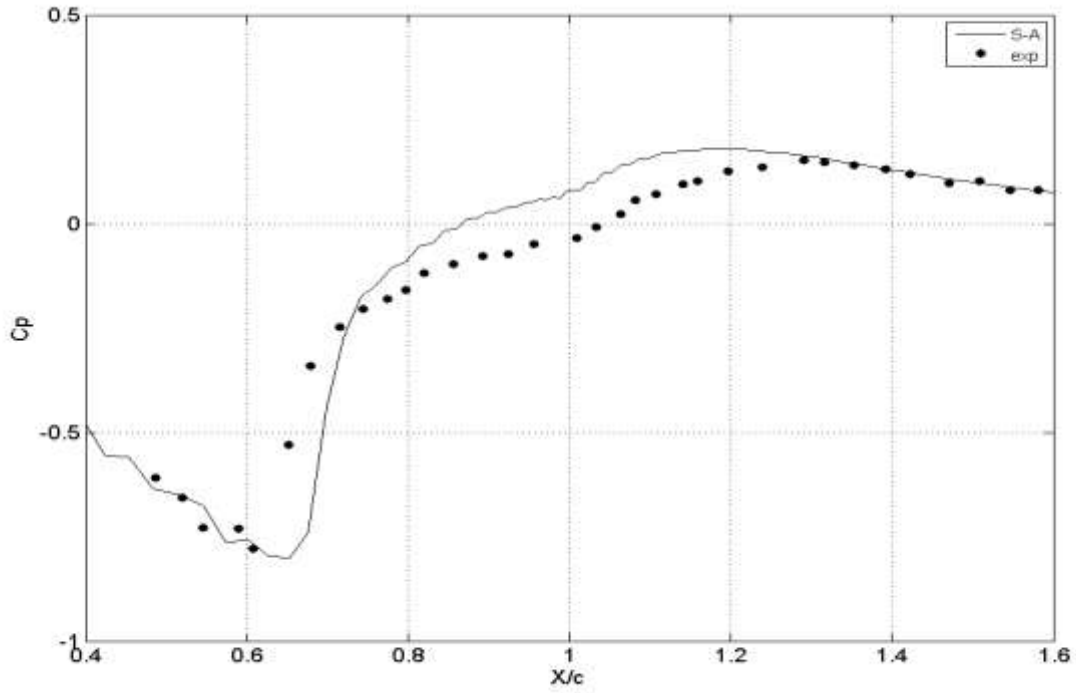

Figure 28: cp comparison with experimental data S-A model

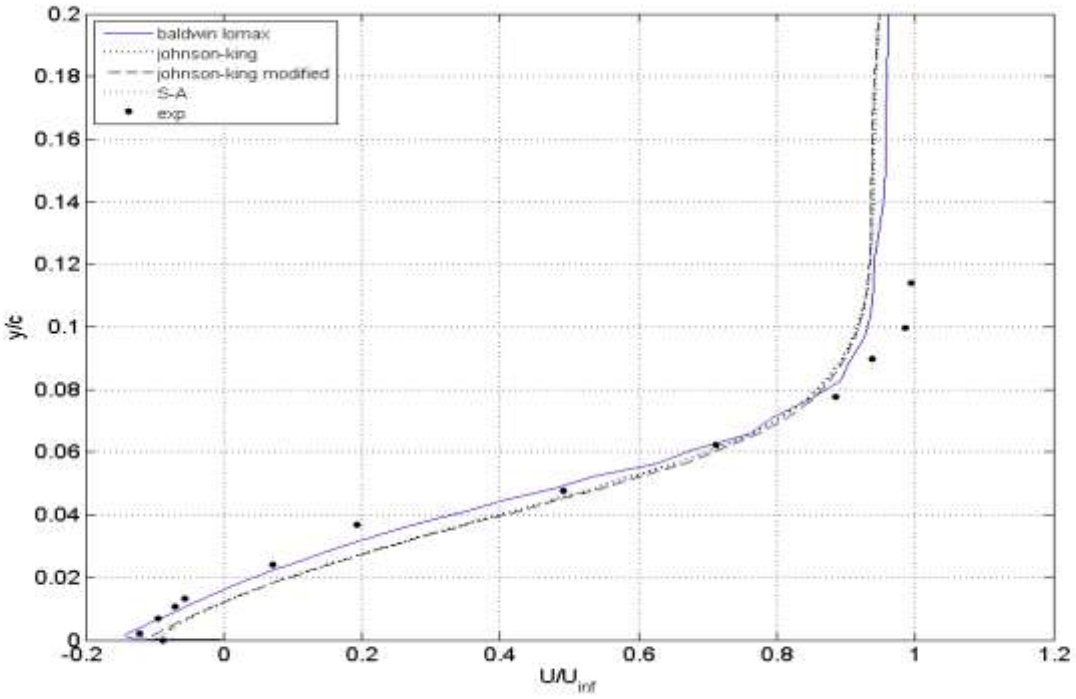

Figure 29: comparison of velocity profiles with experimental data for different models at x=1

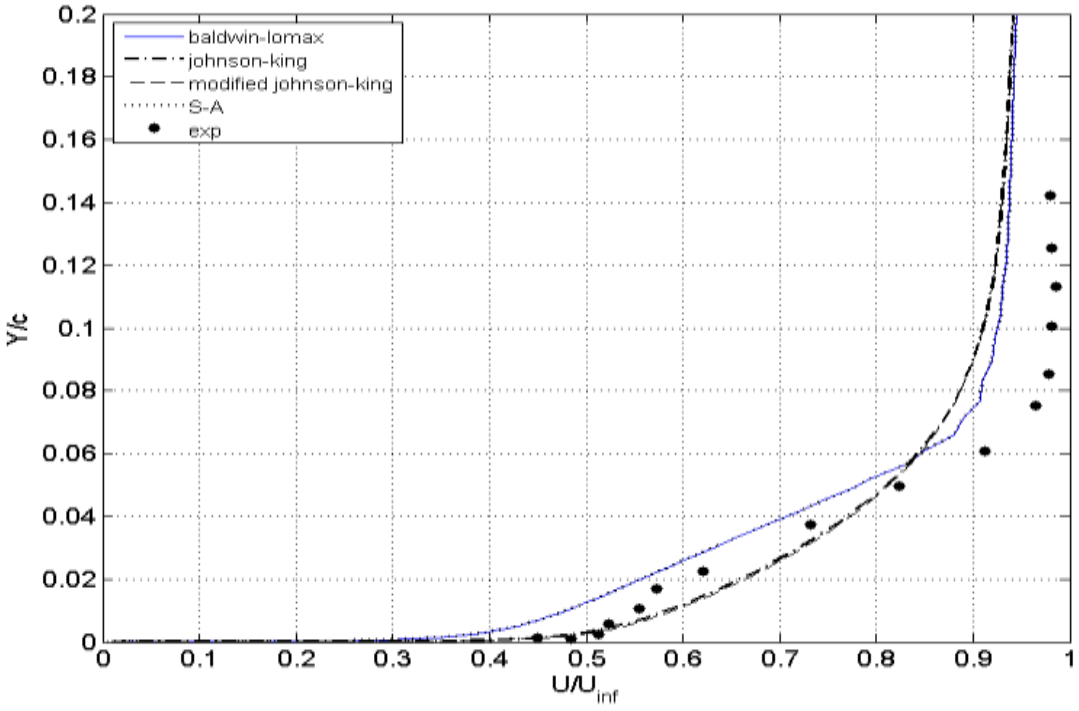

Figure 30: comparison of velocity profiles with experimental profile at x=1.39 for different models

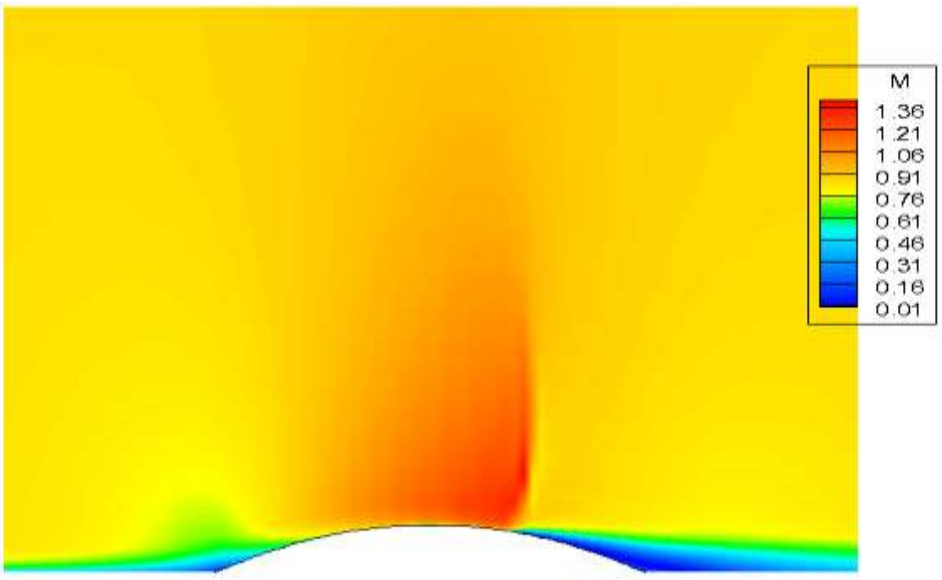

Figure 31: mach no. contours obtained over bump using Baldwin Lomax model

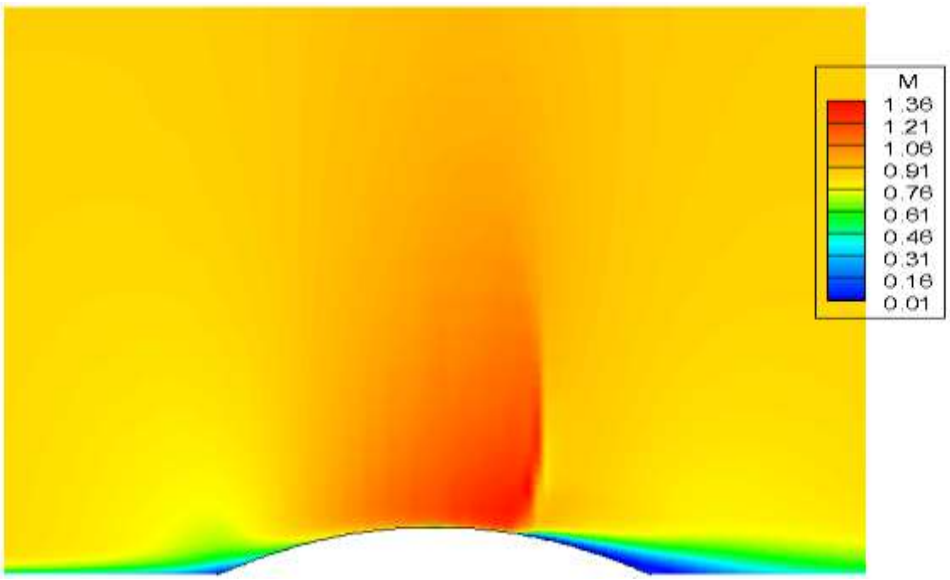

Figure 32Mach no. contours obtained over bump using Johnson-king model

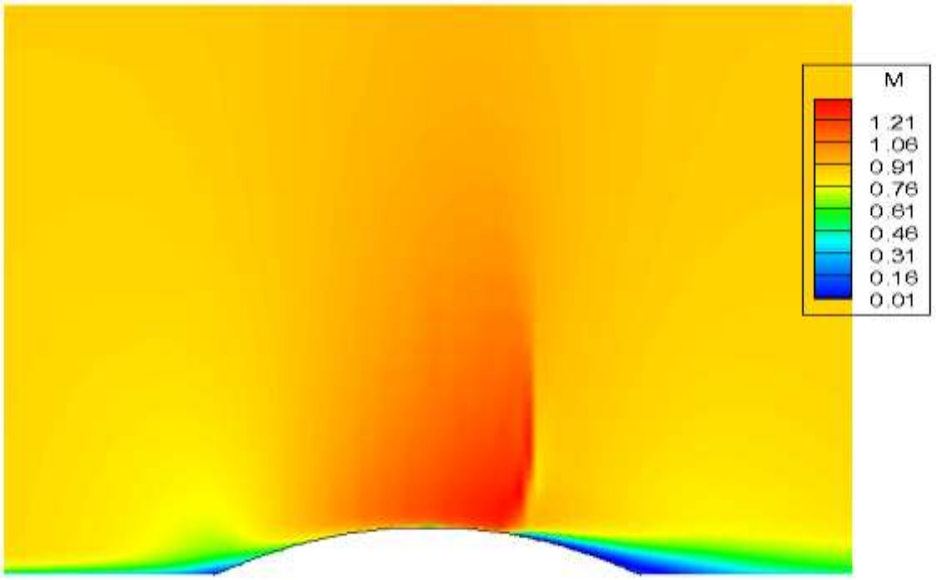

Figure 33: Mach no. contours obtained over bump using modified Johnson-king model

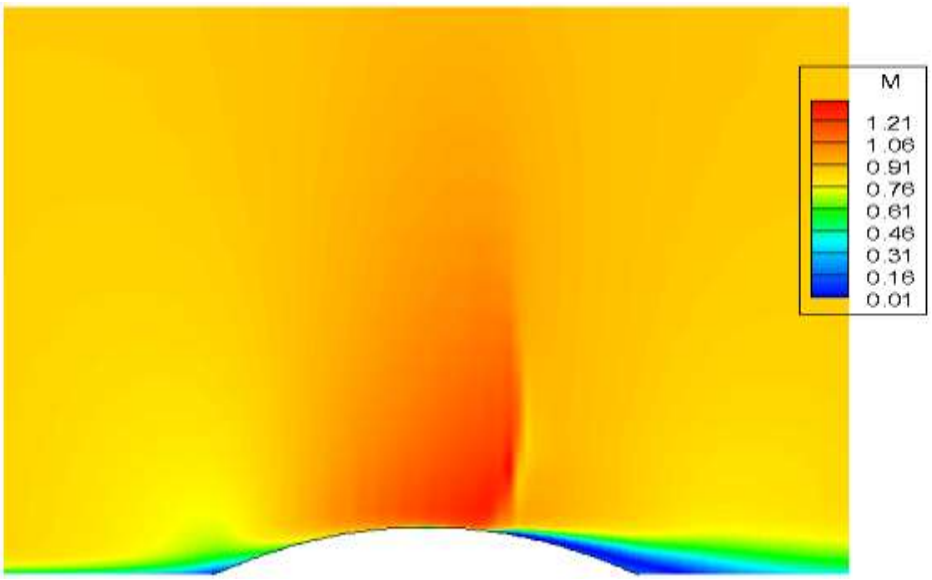

Figure 34: Mach no. contours obtained over bump using Johnson-Abid model

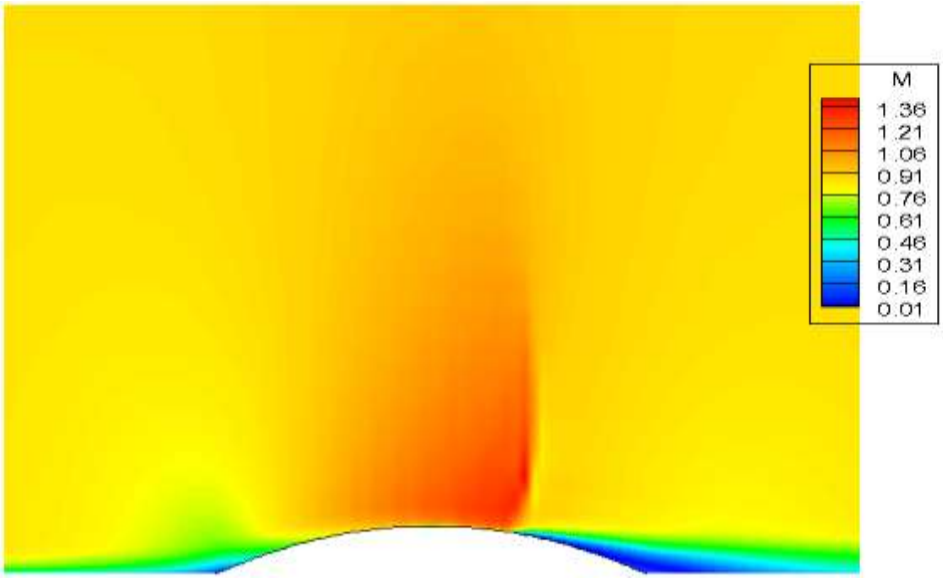

Figure 35: Mach no. contours obtained over bump using S-A model

Figure 29 and 30 show the comparisons of velocity profiles obtained from simulation to that of experimental results. Figures. 31 to 35 are the mach no contours obtained from simulations, which show the prediction of normal shock wave and flow separation bubble for different models. The difference in the separation and reattachment points predicted by different models can be seen in the Mach no. contours. In the both the validation cases computational solutions are in good agreement with experimental results

4.2.4 Results obtained using chein's K-epsilon model:

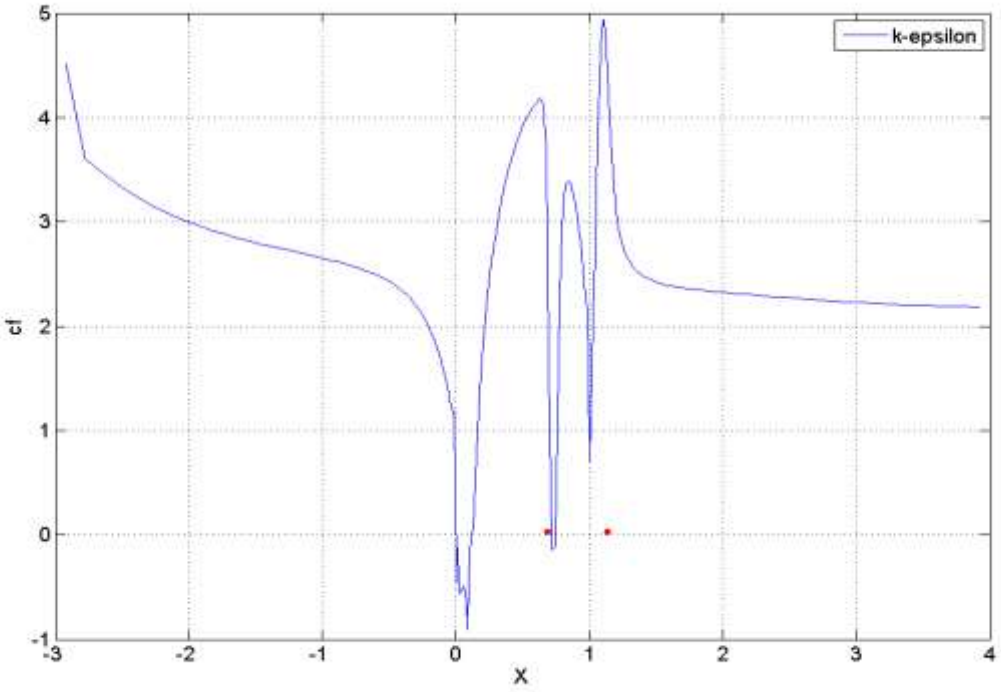

Figure 36: variation of Cf along the bump obtained using chein's k-epsilon model

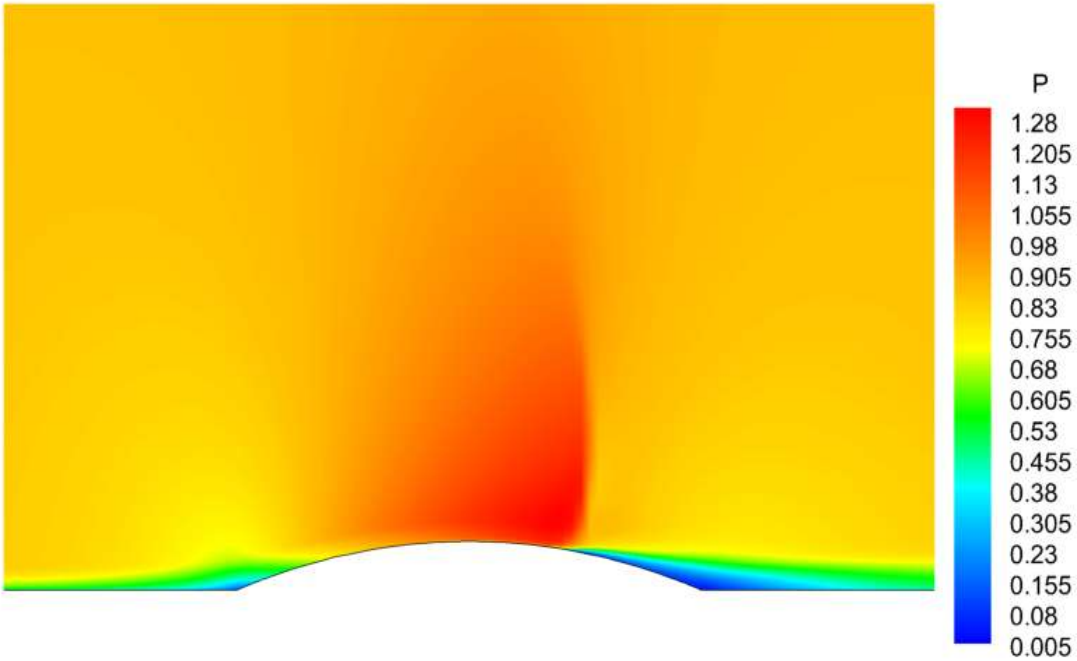

Figure 37: Mach no. contour over the bump obtained using chein's k-epsilon model

The Chien's *k-ε* turbulence model has been used to predict the transonic flow over an axisymmetric bump. 3rd order accurate up-winding has been used to predict the results. The value of the average 'Cd' of the model has (1.113E-01) come very close to the value predicted by other models, but the solution was showing some oscillations. The values of the 'Cf' are found to oscillate over the bump, while it remained constant over the rest of the flow. It has also been mentioned in Ref.[19]. That the Chien's *k-ε* is found have problems with prediction of non-equilibrium separated flow. If has been also been known that *k-ε* models in general have issues with flow separation in non-equilibrium flows (Ref. [10]), Chien's model is found to give very bad solutions. The results have not improved even for the use of exact turbulence kinetic energy and turbulence dissipation rate values. It has also been observed that the *k-ε* model doesn't react properly to the perturbations due to the adverse pressure gradients. This nature can be attributed to the near wall functions that have been added to original model to improve the flow prediction at the walls. The actual model without near wall functions cannot account for the wall effects. As it has been mentioned before, *k-ε* is very sensitive to perturbations in the flow, and hence the solution was oscillating. Damping functions or limiters can be added to the algorithm to make it more stable. Other implementations like a two layered *k-ε* model, which uses a simple mixing length for the eddy viscosity in the vicinity of the wall, which has been found to marginally improve the results. Use of RNG *k-ε* model with two layers is known to have given better solutions [Ref.10]. Implementation of ω (specific dissipation rate) instead of ε as a turbulent length scale equivalent alternative, resulting in a *k-* ω model, has been found to give very accurate answers for such flows and is found to more stable.

5. CONCLUSION AND RECOMENDATIONS

Eddy viscosity models like Baldwin Lomax, Johnson-king, Johnson-Abid and two equations k-ε model were implemented. An attempt was made to validate the implemented model against the available experimental results for supersonic flow over a flat plate and transonic flow over a circular arc bump. The results obtained are in good agreement with the experimental results when used for supersonic flow over a flat plate. Transonic flow over a circular arc bump poses severe challenges to the turbulence model. Johnson-king, Baldwin Lomax, modified Johnson-king and Spallart-Allmaras model seem to predict the floe separation on the bump reasonably well with some exceptions of flow reattachment for Johnson-king model. Modified Johnson-king model improved the flow characteristics in the separation region compared to Johnson-king model as expected. In the Johnson and kings model implemented edge of the boundary layer properties were found using the fact that vorticity tends to decrease away from the wall. A much better procedure to find the boundary layer properties can be used to improve the solution in the regions of flow separation. Further grid independence is to be performed for Johnson and king model and its variants. The Chien's k - ε model faced problems with prediction of separated flow. Near wall terms are possibly the source of deficiencies. Implementation of much better near wall terms and two layered near wall treatment (Chen and Patel), use of Yang and Shih k-ε or RNG k-ε by Yakhot, could possibly give better solutions for axisymmetric bump problem. Further validation of the models is needed for different cases to establish the implementation's reliability.

6. APPENDIX-I

EFFECT OF GRID SPACING ON COEFFICIENT OF SKIN FRICTION AND STANTON NUMBER:

An analysis is carried out on Baldwin-Lomax and Spalart – Allmaras turbulence model to find out the effect of the first length of the grid on skin-friction coefficient. Grids with first length 1, 5, 10, 20 micron are considered and analysis has been done on flat plate model discussed earlier in the report.

It has been observed that as the first length increases, (Coarser grid) the skin friction increased in both Baldwin-Lomax and Spalart - Allmaras model. The coarser grids were unable to capture the gradients properly, resulting in higher velocity gradients and hence higher skin friction coefficient. There is very little change in the skin friction for 1 and 5micron first cell thickness. It can be inferred that the values of gradients converge and the grid is able to capture gradients properly. Any further refinement of the grid is not needed and the 5micron grid can be used for computation.

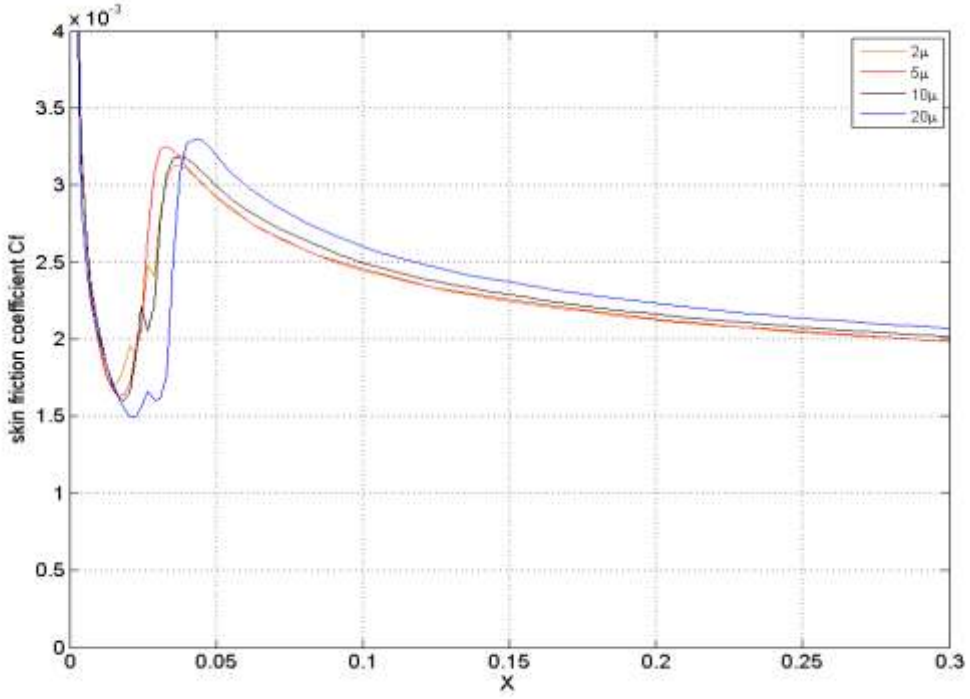

Figure 38: variation of Cf using Baldwin Lomax for different first lengths.

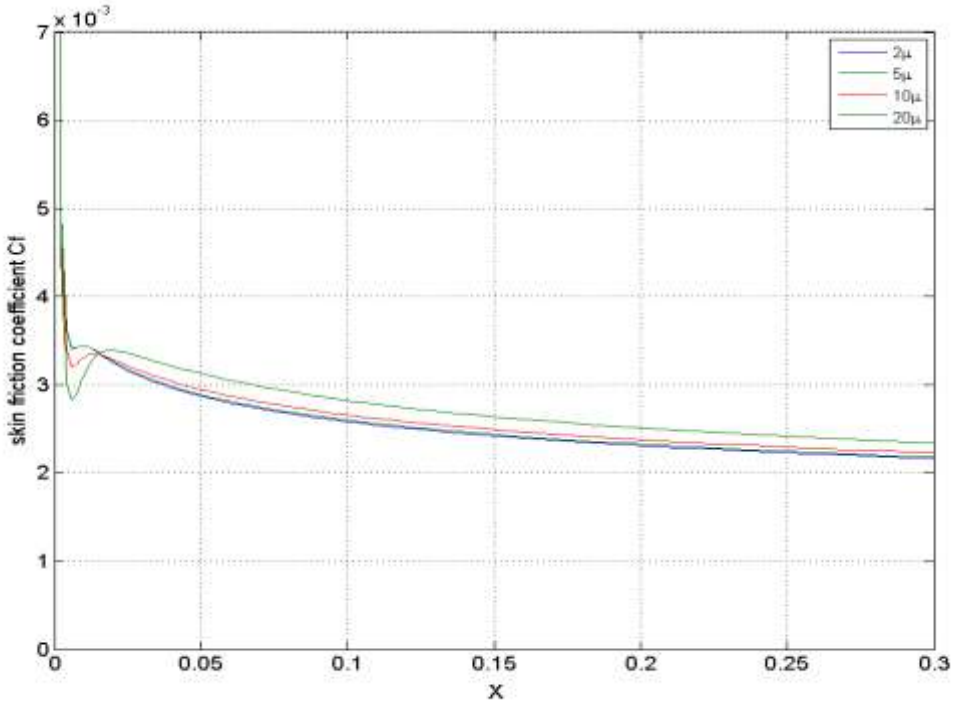

Figure 39: variation of Cf using S-A for different first lengths.

7. REFERENCES

[1]Unnikrishnan, C. and Balu, R., "Development of an Unsteady Navier Stokes Solver for Aerospace Applications," *VSSC. TR.355:95*, Aeronautics Entity, Vikram Sarabhai Space Centre, India, 1995.

[2] TimoSiikonen and JaakkoHoffren, "FINFLO: A Finite-Volume Based Computer Program for Two-Dimensional and Axisymmetric Compressible Flow," *Report No. B-19, Series B*, Helsinki University of Technology, Laboratory of Aerodynamics, Otaniemi, 1989.

[3] TimoSiikonen, Petri Kaurinkoski and SeppoLaine, "Transonic Flow over a Delta Wing using $k - \varepsilon$ Turbulence Model," *ICAS-94-2.3.2*, Helsinki University of Technology, Finland, 1994.

[4] Baldwin, B.L., and Lomax, H., "Thin Layer Approximation and Algebraic Model for Separated Turbulent Flows," *AIAA 78-257*,NASA Ames Research Center, Moffett Field, California, United States of America, 1978.

[5] Spalart, P.R., Allmaras, S.R., "A One-Equation Turbulence Model for Aerodynamic Flows," *AIAA-92-0439*, Boeing Commercial Airplane Group, Seattle, WA 98214-2207, United States of America, 1992.

[6] Johnson, D.A., King, L.S., "A Mathematically Simple Turbulence Closure Model for Attached and Separated Turbulent Boundary Layers," *AIAA 84-0175*, NASA Ames Research Center, Moffett Field, California, United States of America, 1984.

[7] Pappas, C.C., "Measurement of Heat Transfer in the Turbulent Boundary Layer on a Flat Plate in Supersonic Flow and Comparison with Skin-Friction Results," *NACA TN – 3222*, National Advisory Committee for Aeronautics, United States of America.

[8] Goldberg, U., "Hypersonic Flow Heat Transfer Prediction Using Single Equation Turbulence Models," *DOI:10.1115/1.1337653, Journal of Heat Transfer, Vol.123*, Metacomp Technologies, Inc. ,650 Hampshire Road, No.200, Westlake Village, CA91361, United States of America, 2001.

[9] Reece E. Neel, "Advances in Computational Fluid Dynamics: Turbulent Separated Flows and Transonic potential flows," Virginia Polytechnic Institute and State University, Blacksburg, Virginia, 1997.

[10] Hassan Raiesi, UgoPiomelli and Andrew Pollard., "Evaluation of Turbulence Models Using Direct Numerical and Large-Eddy Simulation Data", *DOI:10.1115/1.4003425*, Journal of Fluids Engineering, Vol.133, Department of Mechanical and Material Engineering, Queen's University, Kingston, Canada, February 2011.

[11] Christopher L. Rumsey and Veer N. Vatsa, "A Comparison of the Predicitive Capabilities of Several Turbulence models using upwind and Central-Difference Computer Codes," *AIAA 93-0192,* NASA Langley Research Center, Hampton, Virginia 23681-0001, 1993.

[12]Tao Du and Zi-Niu Wu, "Mixed Analytical/Numerical Method for Low-Reynolds-Number *k-ε* Turbulence Models," *AIAA-2426-337,AIAA Journal Vol. 42 No.6,* Tsinghua University, 100084 Beijing, People's Republic of China, June 2004.

[13] David C. Wilcox, "Turbulence Modeling for CFD," DCW Industries, Inc., La Canada, California, 1994, Pages 23-163.

[14] Lars Davidson, "An Introduction to Turbulence Models," Publication 97/2, Department of Thermo and Fluid Dynamics, Chalmers University of Technology, Goteborg, Sweden, February 24,2011.

[15] Tennekes, H. and Lumley, J.L., *A First Course in Turbulence*, The MIT Press, Massachusetts and London, England, 1972.

[16] John D. Anderson, JR., "Computational Fluid Dynamics: The basics with Applications," McGraw-Hill International Editions - Mechanics Engineering Series, Singapore, 1995.

[17] Ion Paraschivoiu, "Wind Turbine Design with emphasis on Darrieus concept," Polytechnic International Press, 2002, Pages 114-120

[18] Agarwal, R.K. and Gielda, T.P., "Aerodynamics Technology: Volume 1: Final Report, Task1, Three Dimensional Euler/Navier Stokes Aerodynamics Method (TEAM) Enhancements," *WL-TR-93-3010, Volume I,* McDonnell Douglas, St. Louis, July 1994.

[19] Yaras,M.I., Grosvenor, A.D., "An Evaluation of Low Reynolds Number Turbulence Models Part-1, Flat-Plate Boundary layer and Axisymmetric separated flows,", Department of Mechanical and Aerospace Engineering, Carlton University, Ottawa, Canada,2002.